Cell Stem Cell

Article

Activation of hypothalamic-enhanced adult-born neurons restores cognitive and affective function in Alzheimer's disease

Graphical abstract

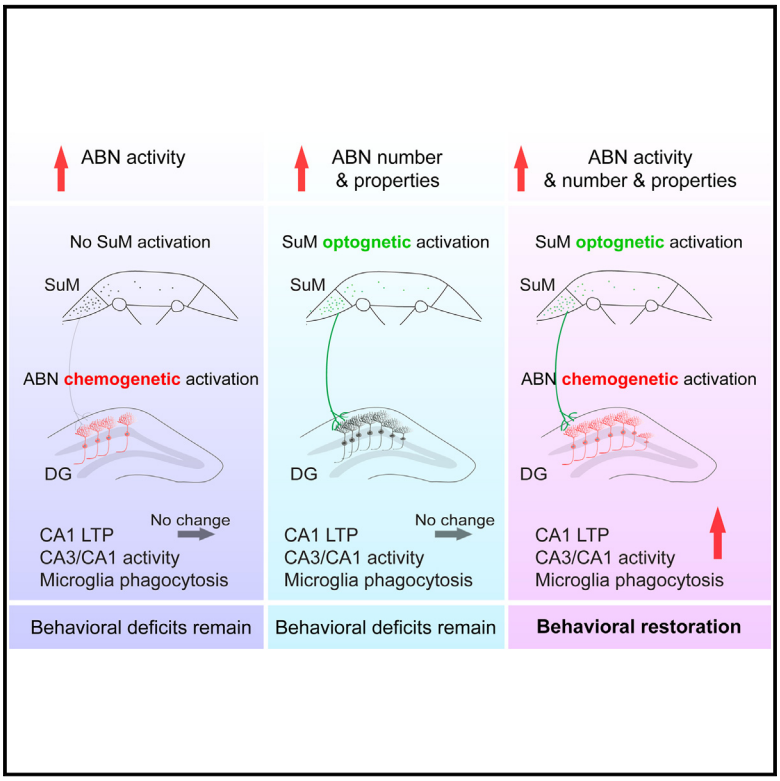

Authors

Ya-Dong Li, Yan-Jia Luo, Ling Xie, ..., Leon G. Coleman, Jr., Xian Chen, Juan Song

Correspondence

juansong@email.unc.edu

In brief

The process of generating adult-born neurons (ABNs) in the hippocampus is impaired in AD. Song and colleagues report a circuit-based strategy by stimulating SuM to enhance hippocampal neurogenesis in AD mice. Activation of SuM-modified ABNs restores cognitive and affective function along with improved hippocampal plasticity and microglia dynamics.

Highlights

- Patterned optogenetic stimulation of SuM enhances hippocampal neurogenesis in AD
- Activation of SuM-enhanced ABNs rescues memory and emotion deficits in AD
- Activation of SuM-enhanced ABNs promotes hippocampal plasticity and activity in AD
- Activation of SuM-enhanced ABNs increases microglia phagocytosis of plaques in AD

Li et al., 2023, Cell Stem Cell *30*, 415–432
April 6, 2023
https://doi.org/10.1016/j.stem.2023.02.006

CellPress

Cell Stem Cell

CellPress

Article

Activation of hypothalamic-enhanced adult-born neurons restores cognitive and affective function in Alzheimer's disease

Ya-Dong Li,[1,2,6] Yan-Jia Luo,[1,2,6] Ling Xie,[3] Dalton S. Tart,[1,7] Ryan N. Sheehy,[1,4,7] Libo Zhang,[1] Leon G. Coleman, Jr.,[1,5] Xian Chen,[3] and Juan Song[1,2,8,*]

[1]Department of Pharmacology, University of North Carolina at Chapel Hill, Chapel Hill, NC 27599, USA
[2]Neuroscience Center, University of North Carolina at Chapel Hill, Chapel Hill, NC 27599, USA
[3]Department of Biochemistry and Biophysics, University of North Carolina at Chapel Hill, Chapel Hill, NC 27599, USA
[4]Pharmacology Curriculum, University of North Carolina at Chapel Hill, Chapel Hill, NC 27599, USA
[5]Bowles Center for Alcohol Studies, University of North Carolina at Chapel Hill, Chapel Hill, NC 27599, USA
[6]These authors contributed equally
[7]These authors contributed equally
[8]Lead contact
*Correspondence: juansong@email.unc.edu
https://doi.org/10.1016/j.stem.2023.02.006

SUMMARY

Patients with Alzheimer's disease (AD) exhibit progressive memory loss, depression, and anxiety, accompanied by impaired adult hippocampal neurogenesis (AHN). Whether AHN can be enhanced in impaired AD brain to restore cognitive and affective function remains elusive. Here, we report that patterned optogenetic stimulation of the hypothalamic supramammillary nucleus (SuM) enhances AHN in two distinct AD mouse models, 5×FAD and 3×Tg-AD. Strikingly, the chemogenetic activation of SuM-enhanced adult-born neurons (ABNs) rescues memory and emotion deficits in these AD mice. By contrast, SuM stimulation alone or activation of ABNs without SuM modification fails to restore behavioral deficits. Furthermore, quantitative phosphoproteomics analyses reveal activation of the canonical pathways related to synaptic plasticity and microglia phagocytosis of plaques following acute chemogenetic activation of SuM-enhanced (vs. control) ABNs. Our study establishes the activity-dependent contribution of SuM-enhanced ABNs in modulating AD-related deficits and informs signaling mechanisms mediated by the activation of SuM-enhanced ABNs.

INTRODUCTION

Alzheimer's disease (AD) is characterized by the formation of β-amyloid (Aβ) plaques and neurofibrillary tangles, neuroinflammation, and neurodegeneration.[1,2] Spatial memory decline, depression, and anxiety are known to be early clinical signs of AD,[3,4] in which the hippocampus has a crucial role.[2,5] Within the hippocampus, the dentate gyrus (DG) contains neural stem cells that continue to generate adult-born neurons (ABNs) throughout life, a process known as adult hippocampal neurogenesis (AHN). Substantial evidence has supported the existence of AHN in human brains and the level of AHN declines significantly during AD progression.[6–12] Ample studies using rodent models have established the causal role of ABNs in regulating memory performance[13–18] and emotional states,[18,19,20] two key functions of the adult hippocampus that are impaired in AD patients. However, the function and therapeutic potential of ABNs in AD brains remains largely unknown. A long-standing question centers on whether AHN can be effectively enhanced in otherwise impaired AD brains and exploited for therapeutic purpose in AD to restore hippocampal function.

It has been well-established that environmental stimuli, such as an enriched/novel environment and voluntary exercise, can enhance AHN and improve hippocampal function in both healthy and AD mice, potentially through mechanisms involved in neurotrophic factors (i.e., BDNF, brain-derived neurotrophic factor) or microRNAs.[21–26] However, environmental stimuli exert broad effects on various brain regions and cell types, so the key circuit and signaling mechanisms that mediate enhanced AHN and improved hippocampal function in these contexts remain largely undefined. Given that dysregulated circuits and networks are the hallmarks of AD, lacking circuit-based knowledge represents one of the major roadblocks for clinical transformation to leverage the beneficial effects associated with environmental stimulations to improve AHN and brain functions. A series of our studies have established that AHN is dynamically regulated by activity mediated by diverse neural circuits.[22,27–31] Importantly, neural circuits are capable of relaying external stimuli to the neurogenic niche to regulate AHN.[27] Recently, we identified a key subcortical region in the hypothalamus, the supramammillary nucleus (SuM), which sends abundant projections to the DG and is highly responsive to pro-neurogenic stimuli.[22]

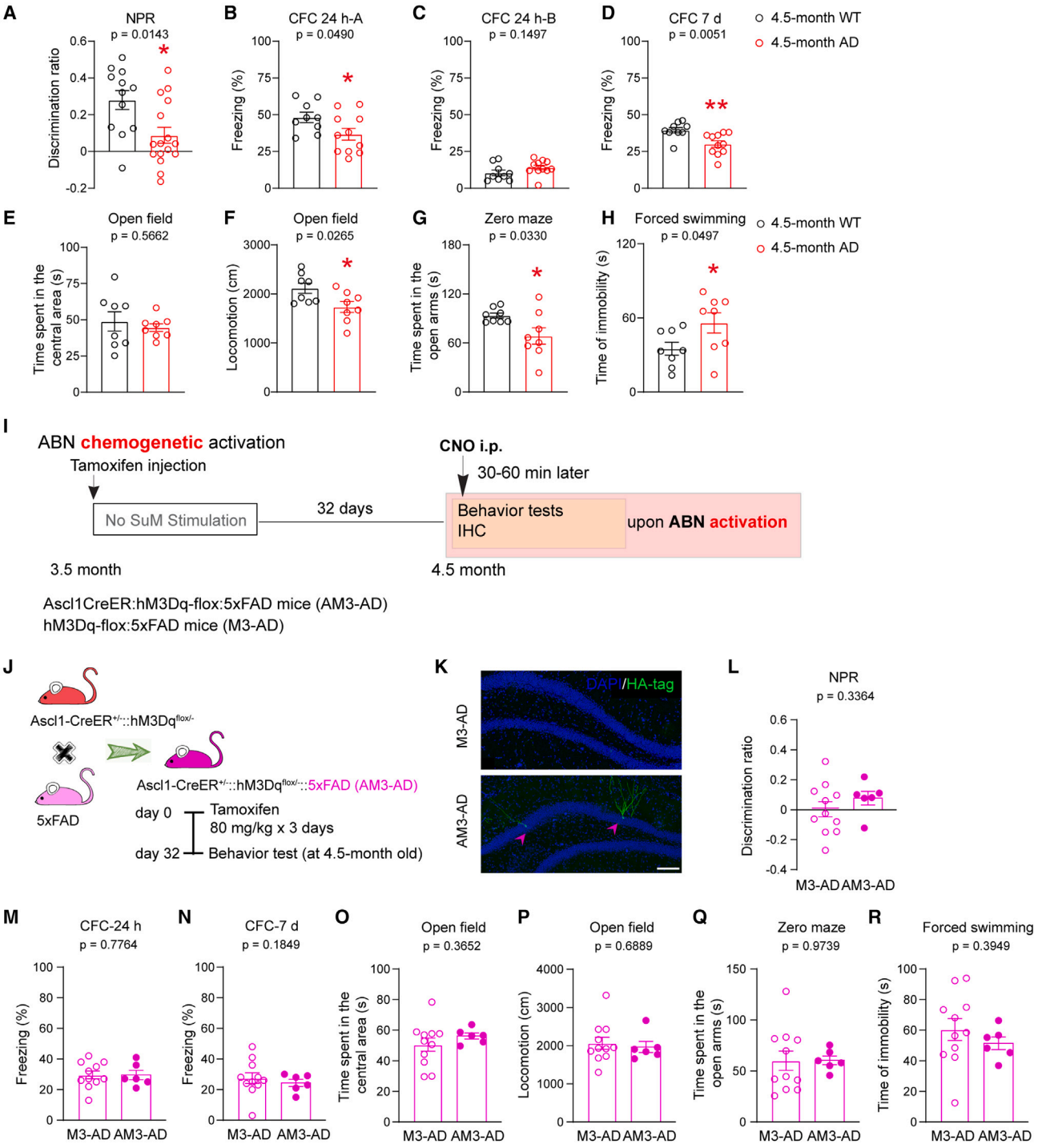

Figure 1. Chemogenetic activation of ABNs fails to rescue cognitive and emotional deficits in 5×FAD mice

(A) Discrimination ratio in the NPR test in 4.5-month-old WT/AD mice. n = 12 mice for WT group, and n = 16 mice for AD group.

(B–D) Freezing time in context A at 24 h (B), in context B at 24 h (C), and in context A at 7 days (D) in the CFC test. n = 9 mice for WT group, n = 11 mice for AD group.

(E–H) Affective behavior tests in 4.5-month-old WT/AD mice. Time spent in center area (E) and total locomotion (F) in the open field test. Time spent in open arms in the zero maze test (G). Time of immobility in the forced swimming test (H). n = 8 mice for each group.

(I) Experimental scheme. Tamoxifen was injected into 3.5-month-old Ascl1CreER:hM3Dq:5×FAD (AM3-AD) or hM3Dq:5×FAD (M3-AD) mice. Behavioral tests were performed 32 days later with the intraperitoneal (i.p.) injection of CNO to activate ABNs in 4.5-month-old AD mice.

(J) Experimental scheme for chemogenetic activation of ABNs at 32 days post injection (dpi) in 4.5-month-old AM3-AD mice.

(K) Sample images showing expression of HA+ hM3Dq cells in the DG of AM3-AD mice, but not M3-AD mice. Scale bars, 100 μm.

(L) Discrimination ratio in the NPR test following chemogenetic activation of ABNs. n = 11 mice for M3-AD group, and n = 6 mice for AM3-AD group.

(legend continued on next page)

Specifically, SuM neurons exhibit increased firing frequency, calcium dynamics, and c-Fos expression when animals are exposed to a novel environment. Importantly, SuM neurons are required for environmental novelty (EN)-induced enhancement of AHN, as ablation of SuM neurons abolishes these effects. These findings raise an exciting possibility that stimulating the SuM may mimic EN-induced enhancement of AHN.

Supporting this view, we found that patterned optogenetic stimulation of SuM neurons at the frequency mimicking their firing rate in the novel environment increases the number of behaviorally relevant ABNs with enhanced developmental properties.[22] Strikingly, acute chemogenetic activation of a small population of time-stamped SuM-enhanced ABNs improves memory performance and reduces anxiety-like behavior. These results suggest that increasing activity of SuM-enhanced ABNs, even just a small number, can convey significant behavioral benefits.

In this study, we set out to test this novel AHN-enhancing strategy in degenerated AD brains and address whether it can restore AHN and achieve functional recovery using two distinct AD mouse models, 5×FAD[32] and 3×Tg-AD.[33] We found that patterned optogenetic stimulation of SuM in AD mice at various disease stages (ranging from early to late) restores the number and developmental properties of ABNs. Importantly, acute chemogenetic activation of a small population of SuM-enhanced ABNs in AD mice can restore memory and reduce anxiety/depression-like behaviors. By contrast, SuM stimulation alone or acute activation of ABNs without SuM modification fails to restore behavioral deficits in AD mice. To probe ABN-activity-dependent mechanisms, we performed quantitative phosphoproteomics of the hippocampus following acute chemogenetic activation of SuM-enhanced ABNs. Our analyses revealed activation of the canonical pathways related to synaptic plasticity and microglia phagocytosis of plaques in response to acute activation of SuM-enhanced ABNs.

RESULTS

Impaired hippocampal neurogenesis occurs prior to behavioral deficits in 5×FAD mice

We first examined hippocampal neurogenesis and behavioral states in relation to plaque deposition at various ages of 5×FAD mice and their littermate wild-type (WT) controls. First, we examined plaque deposition in the DG where AHN occurs and found no Aβ plaque deposition in 2.5-month-old 5×FAD mice. Mild plaque deposition was found in 3.5-month-old AD mice, which became progressively more severe at 4.5 and 6.5 months old. By contrast, no plaques were found in littermate WT controls at these stages (Figure S1A).

We then examined when AHN impairment in 5×FAD mice started. Interestingly, the density of Ki67+ cells was significantly reduced in 3.5-month-old (but not 2.5-month-old) 5×FAD mice without altering the density of DCX+ immature neurons (Figures S1B–S1E and S2A–S2D). These results suggested that AHN impairment started in 3.5-month-old 5×FAD mice, and at this time only the proliferation of neural precursor cells was affected. To address whether reduced proliferation leads to reduced production of ABNs, we performed lineage tracing of neural stem/progenitor cells (NSPCs) in 3.5- and 5.5-month-old 5×FAD and WT mice to evaluate the production of behaviorally relevant ABNs during the critical window of 4–6 weeks[34,35] (Figures S1F and S1K). To label NSPCs in AD mice, we generated triple transgenic mice harboring Ascl1-CreERT2 (a Cre-inducible recombinase under the control of the endogenous achaete-scute homolog 1 promoter[36]), Ai9 (a floxed reporter line expressing tdTomato[37]), and 5×FAD, referred to as Ascl1-Ai9-AD mice. The double transgenic littermates (Ascl1-CreER::Ai9) were used as controls, and referred to as Ascl1-Ai9 mice. With 3-day tamoxifen (TMX) induction, a significant reduction in the densities of Ki67+ tdTomato+ and total tdTomato+ cells was observed in both the 3.5- and 5.5-month-old (but not the 2.5-month-old) Ascl1-Ai9-AD mice (Figures S1G–S1J, S1Q–S1S, and S2E–S2H). 32 days after the first TMX induction, when tdTomato+ cells reached the critical window for behavioral contribution, a significant reduction of total tdTomato+, DCX+ tdTomato+, NeuN+ tdTomato+, and DCX+ cells was observed in 4.5- and 6.5-month-old Ascl1-Ai9-AD mice as compared with their age-matched controls (Figures S1L–S1P, S1T–S1W, and S2I) without altering the DG volume (Figures S2J–S2M).

We further examined hippocampus-dependent memory performance and emotional states of 3.5- and 4.5-month-old 5×FAD mice to determine when these behaviors become impaired. Novel place recognition (NPR) and contextual fear conditioning (CFC) were performed to assess memory performance, open field and elevated zero maze were performed to assess anxiety-like behavior, and forced swimming was performed to assess depression-like behavior. These behaviors were selected, as we recently showed that they respond to acute chemogenetic manipulation of ABNs during the critical window in WT mice,[22] thus are ABN-activity dependent. As a result, 4.5-month-old 5×FAD mice exhibited a decreased discrimination ratio in the NPR test (Figure 1A) and a decreased freezing time in context A (24 h and 7 days after foot shocks) in the CFC test (Figures 1B and 1D) without altering the freezing time in the neutral context B (Figure 1C). In addition, the time spent in the central area of the open field was not altered (Figure 1E) but the total locomotion was decreased (Figure 1F). Furthermore, the time spent in the open arms of the elevated zero maze was decreased (Figure 1G), and the time of immobility in the forced swimming test was increased (Figure 1H). By contrast, 3.5-month-old 5×FAD mice showed no significant changes in all the behaviors tested above (Figures S3A–S3H). These results revealed impaired memory and elevated anxiety- and depression-like behavior in 4.5-month-old (but not 3.5-month-old) 5×FAD mice. Therefore, AHN deficits occurred (3.5 months old) before behavioral deficits (4.5 months old) in 5×FAD mice.

(M and N) Freezing time in context A at 24 h (M) and 7 days (N) in CFC test. n = 11 mice for M3-AD group, and n = 6 mice for AM3-AD group.
(O–R) Affective behavior tests following chemogenetic activation of ABNs. Time spent in center area (O) and total locomotion (P) in the open field test. Time spent in open arms in the zero maze test (Q). Time of immobility in the forced swimming test (R). n = 11 mice for M3-AD group, and n = 6 mice for AM3-AD group.
Data are represented as mean ± SEM. *$p < 0.05$, **$p < 0.01$ by unpaired t test.
See also Figures S1–S3.

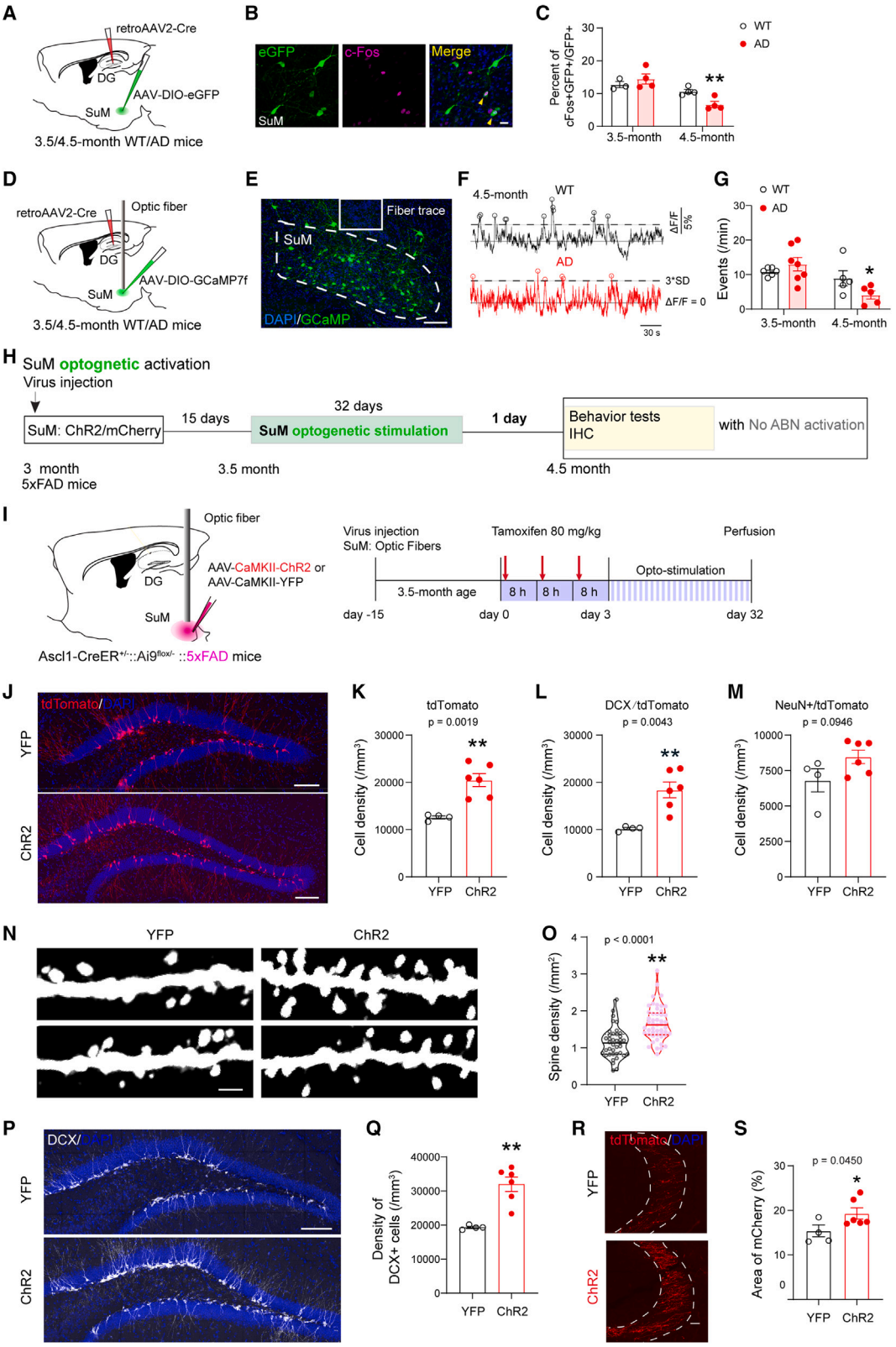

Figure 2. Chronic patterned optogenetic activation of SuM leads to increased ABNs with improved developmental properties in 5×FAD mice

(A) Experimental scheme for c-Fos quantification in DG-projecting SuM neurons.

(B) Representative images of c-Fos expression in DG-projecting SuM neurons. Arrowheads indicate c-Fos+GFP+ cells. Scale bars, 20 μm.

(legend continued on next page)

Activation of ABNs fails to rescue behavioral deficits in 5×FAD mice

Our recent study showed that the acute chemogenetic activation of ABNs during the critical window of 4–6 weeks improves memory performance and emotional sates in WT mice.[22] Therefore, we asked whether activation of ABNs in 4.5-month-old 5×FAD mice could restore these cognitive and affective behaviors. To activate ABNs, we generated triple transgenic mice harboring Ascl1-CreER, floxed hM3Dq,[38] and 5×FAD, referred to as AM3-AD mice. The double transgenic hM3Dq::5×FAD mice were used as controls, referred to as M3-AD mice. These mice were induced with TMX for 3 consecutive days, and 32 days after the first TMX injection, cognitive and affective behaviors mentioned above in Figures 1A–1H were performed upon acute chemogenetic activation of ABNs by intraperitoneal injection of clozapine-*N*-oxide (CNO) (Figures 1I and 1J). Note, HA+ hM3Dq+ ABNs were found in AM3-AD (but not M3-AD control) mice (Figure 1K), thus validating the reliability of Cre-induced expression of hM3Dq. As a result, chemogenetic activation of ABNs in 4.5-month-old AM3-AD mice had no effects on all the behaviors tested, including NPR (Figure 1L), CFC (Figures 1M and 1N), open field (Figures 1O and 1P), elevated zero maze (Figure 1Q), and forced swimming (Figure 1R). These results suggested that the activation of impaired ABNs in the diseased AD brain does not convey behavioral benefits.

Patterned optogenetic stimulation of SuM enhances hippocampal neurogenesis in 5×FAD mice

Our recent study identified a key subcortical region in the hypothalamus, the SuM, which upon patterned optogenetic stimulation can effectively enhance AHN by acting on multiple neurogenesis stages, leading to an increased number of behaviorally relevant ABNs with enhanced developmental properties, including increased maturity, longer/more elaborate dendrites, and increased dendritic spines in WT mice.[22] Based on these findings, we asked whether patterned optogenetic stimulation of SuM neurons can similarly enhance ABNs in AD mice.

To address this question, we first examined the activity of DG-projecting SuM neurons in 5×FAD mice measured by c-Fos expression and Ca^{2+} dynamics of DG-projecting SuM neurons in 5×FAD and WT mice at 3.5 and 4.5 months of age. To label DG-projecting SuM neurons, retroAAV-Cre was injected into the DG, and AAV-DIO-eGFP (for c-Fos quantification) or AAV-DIO-GCaMP7f (for fiber photometry recording) was injected into the SuM (Figures 2A and 2D). A significant reduction of c-Fos expression and Ca^{2+} activity in DG-projecting SuM neurons was found in 4.5-month-old (but not 3.5-month-old) 5×FAD mice (Figures 2B, 2C, and 2E–2G). These results suggested that DG-projecting SuM neurons exhibit reduced activity in 4.5-month-old (but not 3.5-month-old) 5×FAD mice.

We then applied 32-day patterned optogenetic stimulation of SuM neurons in 3.5-month-old triple transgenic Ascl1-Ai9-AD mice injected with AAV-CaMKII-ChR2-YFP or AAV-CaMKII-YFP in the SuM, referred to as ChR2-AD (experimental) or YFP-AD (control) mice (Figures 2H and 2I), followed by the quantification of the number and developmental properties of SuM-modified and control ABNs in 4.5-month-old ChR2- and YFP-AD mice (Figures 2H and 2I). The SuM stimulation paradigm has been used and validated in WT mice from our recent study.[22] By combining SuM stimulation and Cre-inducible triple transgenic AD mice, we can study a cohort of time-stamped ABNs that have been modified by SuM stimulation. Our results showed that chronic patterned opto-stimulation of SuM led to a significant increase in the densities of tdTomato+ and DCX+ tdTomato+ cells, along with an increased trend of NeuN+ tdTomato+ cells ($p = 0.095$) (Figures 2J–2M) and a significant increase in the dendritic spine density of tdTomato+ ABNs (Figures 2N and 2O) in 4.5-month-old ChR2-AD mice as compared with sham control YFP-AD mice. The density of total DCX+ cells (independent of tdTomato fluorescence) in SuM-stimulated ChR2-AD mice was also significantly increased as compared with sham control YFP-AD mice (Figures 2P and 2Q), thus confirming that the neurogenic effects mediated by SuM stimulation were not an artifact of transgene expression in ABNs. Interestingly, the mossy fiber axons of tdTomato+ ABNs in the CA3 subfield of ChR2-AD mice were significantly increased (Figures 2R and 2S), indicating increased connectivity between SuM-enhanced ABNs and CA3 neurons. Notably, SuM stimulation did not alter Aβ plaque pathology and GFAP expression (proxy for neuroinflammation) in the DG of ChR2-AD mice (Figures S4A–S4C). Moreover, c-Fos expression in the DG,

(C) Percent of c-Fos expression in DG-projecting SuM neurons. n = 3–4 mice in each group.
(D) Experimental scheme for calcium recording of DG-projecting SuM neurons.
(E) Sample image showing GCaMP expression in DG-projecting SuM neurons and fiber implantation. Scale bars, 100 μm.
(F) Representative traces of population calcium activity in DG-projecting SuM neurons.
(G) Events of population calcium activity in DG-projecting SuM neurons. n = 5–7 mice in each group.
(H) Experimental scheme. Optogenetic activation of SuM to enhance ABNs. Following viral injection to label SuM with ChR2/mCherry, optogenetic stimulation of SuM was given to 3.5-month-old AD mice for 32 days to restore impaired ABNs. Behavioral tests were performed 1 day later to avoid acute effect of chronic SuM stimulation.
(I) Lineage tracing in Ascl1-Ai9-AD mice with optogenetic stimulation of SuM for 32 days.
(J) Representative confocal images of tdTomato+ cells in Ascl1-Ai9-AD mice after 32-day SuM stimulation paradigm. Scale bars, 100 μm.
(K–M) Density of tdTomato+ (K), tdTomato+/DCX+ (L), and tdTomato+/NeuN+ (M) cells. n = 4 mice for YFP group, n = 6 mice for ChR2 group.
(N and O) Sample images of dendritic spines (N) and quantification of dendritic spine density (O). Scale bars, 1 μm. 80 dendritic segments from 4 mice for each group.
(P) Representative confocal images of DCX+ cells in the DG. Scale bars, 100 μm.
(Q) Density of DCX+ cells in the DG. n = 4 mice for YFP group, and n = 6 mice for ChR2 group.
(R) Representative images of tdTomato+ terminals of ABNs in the CA3. Scale bars, 100 μm.
(S) Quantification of the area of tdTomato (percent of area) in the CA3. n = 4 mice for YFP group, and n = 6 mice for ChR2 group.
Data are represented as mean ± SEM. *$p < 0.05$, **$p < 0.01$ by unpaired t test or two-way ANOVA, followed by Tukey's post hoc test.
See also Figures S4 and S5.

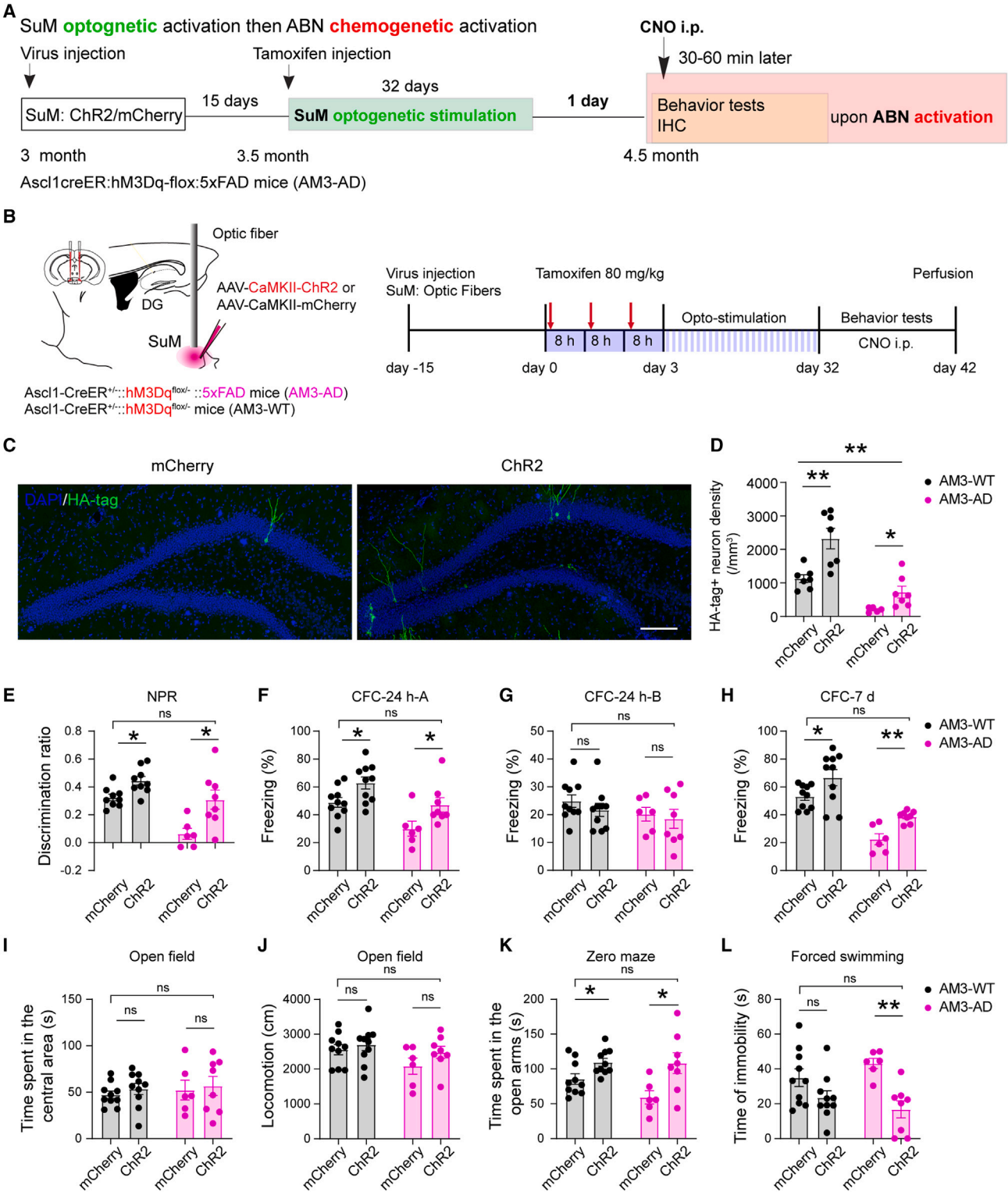

Figure 3. Acute chemogenetic activation of SuM-enhanced ABNs restores cognitive and affective deficits in 5×FAD mice

(A) Experimental scheme. Chemogenetic activation of SuM-enhanced ABNs. Following viral injection to label SuM, tamoxifen was injected and optogenetic stimulation of SuM was given to 3.5-month-old AM3-AD mice for 32 days to restore impaired ABNs. Behavioral tests were carried 1 day later to avoid acute effect from SuM stimulation. Then, CNO i.p. injection was given to 4.5-month-old AM3-AD mice for chemogenetic activation of SuM-modified or control ABNs during behavioral tests.

(B) Experimental scheme for behavioral tests following acute chemogenetic activation of SuM-modified ABNs.

(legend continued on next page)

CA3, and CA1 was not altered (Figures S4D and S4E). These results suggested that SuM stimulation leads to an increased number of ABNs with improved developmental properties without significantly altering AD pathology in the neurogenic niche.

Activation of SuM-enhanced ABNs rescues behavioral deficits in 5×FAD mice

Given that pattered SuM stimulation enhanced AHN in AD mice, we wondered whether SuM-stimulated 5×FAD mice exhibit improved behaviors. Behavioral tests were performed 1 day after chronic SuM stimulation to avoid acute circuit effects (Figure 2H). As a result, no behavioral improvements were observed following chronic SuM stimulation, though these animals have SuM-enhanced ABNs (Figure S5), suggesting that SuM stimulation alone is not sufficient for behavioral improvement in 5×FAD mice. These results are consistent with recent findings that increasing AHN alone failed to ameliorate cognitive deficits in the same 5×FAD mouse model.[24]

We next examined whether the activation of these SuM-enhanced ABNs can restore behavioral deficits in 5×FAD mice. AAV-CaMKII-ChR2-mCherry or AAV-CaMKII-mCherry were injected into the triple transgenic AM3-AD mice, referred to as ChR2-AM3-AD and mCherry-AM3-AD mice. Similar TMX induction and SuM stimulation paradigms were applied in 3.5-month-old 5×FAD mice, followed by behavioral tests (Figures 3A and 3B). Chronic SuM stimulation significantly increased the density of HA+ hM3Dq+ cells in ChR2-AM3-AD mice as compared with mCherry-AM3-AD mice (Figures 3C and 3D). To avoid acute circuit effects from chronic opto-stimulation of SuM, we tested behaviors upon acute chemogenetic activation of SuM-enhanced or control ABNs 1 day after patterned SuM stimulation. Strikingly, acute chemogenetic activation of SuM-enhanced ABNs in ChR2-AM3-AD mice significantly increased the discrimination ratio in the NPR test (Figure 3R) and the freezing time in context A (24 h and 7 days after foot shocks) in the CFC test (Figures 3F and 3H), without altering the freezing time in the neutral context B (Figure 3G). In addition, the time spent in the open arms of the zero maze was significantly increased and the time of immobility in the forced swimming test was significantly decreased (Figures 3K and 3L). By contrast, the time spent in the central area of the open field and locomotion were not significantly altered (Figures 3I and 3J). Notably, animal performance in AD mice reached similar level as AM3-WT mice (Figures 3E–3L), indicative of a full restoration. These results suggested that the activation of SuM-enhanced ABNs rescues both memory and emotion deficits in 5×FAD mice, thus highlighting activity-dependent contribution of SuM-enhanced ABNs in AD brains.

Note, in contrast to most studies trying to label as many ABNs as possible to maximize the chance for behavioral changes, we tuned the TMX dose in our Cre-inducible mice to manipulate a small population of time-stamped ABNs (~300 ABNs/DG, <0.05% of the total DG granule neuron population) at a comparable level of AHN in humans, as the level of AHN in humans is lower than that in mice and is even lower in AD patients. Therefore, these findings suggest that modulating the activity of SuM-enhanced ABNs, even just a small population, can exert profound effects on behaviors in AD brains.

Activation of SuM-enhanced ABNs rescues behavioral deficits in aged 3×Tg-AD mice

The 5×FAD mice exhibit severe plaque deposition at a relatively young age; therefore, a concern was raised regarding the lack of the aging factor critical for AD in this mouse model. To address this issue, we incorporated an additional AD mouse model, 3×Tg-AD, which exhibits much slower AD pathology than 5×FAD mice. We examined neurogenic and behavioral effects mediated by SuM stimulation in 3×Tg-AD mice at 9 and 15 months of age. Specifically, AAV-CaMKII-ChR2-YFP or AAV-CaMKII-YFP was injected into the SuM for optogenetic stimulation of SuM neurons, followed by injection of the mixture of retrovirus expressing Cre (RV-CAG-Cre-HA) and AAV-DIO-hM3Dq-mCherry to the DG for chemogenetic stimulation of ABNs during behavioral tests. A similar 32-day SuM opto-stimulation paradigm was applied in 9- and 15-month-old 3×Tg-AD mice to enhance ABNs (Figure 4A). Consistent with the findings in 4.5-month-old 5×FAD mice, we found that patterned opto-stimulation of SuM increased the density of HA+ ABNs in both 9- and 15-month-old 3×Tg-AD mice (Figures 4B and 4C) without altering the percentage of HA+DCX+/HA+ ABNs (Figure 4D). Moreover, the density of total DCX+ ABNs (independent of fluorescence) in both 9- and 15-month-old 3×Tg-AD mice was also increased following SuM stimulation (Figure 4E), thus confirming that neurogenic effects mediated by SuM stimulation were not an artifact of viral-mediated expression in ABNs. Furthermore, acute chemogenetic activation of SuM-enhanced (but not control) ABNs rescued spatial memory performance in the NPR test and anxiety/depression-like behaviors in the elevated zero maze, open filed, and forced swimming tests in both 9- and 15-month-old 3×Tg-AD mice (Figures 4F and 4H–4J) without affecting locomotion (Figure 4G). These results not only validated the neurogenic and behavioral effects mediated by SuM stimulation in another distinct AD mouse model but also suggested that SuM-mediated AHN-enhancing strategy is effective in aged AD mice.

Phosphoproteomics analyses reveal signaling mechanisms mediated by activation of SuM-enhanced ABNs in 5×FAD mice

These behavioral findings promoted us to address the signaling mechanisms mediated by activation of SuM-enhanced ABNs

(C and D) Representative images showing expression (C) and density (D) of HA-tag+ hM3Dq cells in the DG. Scale bars, 100 μm. n = 5–7 mice for each group.
(E) Discrimination ratio in the NPR test after chemogenetic activation of SuM-enhanced ABNs. For WT mice, n = 9 mice for each group; for AD mice, n = 6 mice for mCherry group, and n = 8 mice for ChR2 group.
(F–H) Freezing time in context A at 24 h (F), in context B at 24 h (G), and in context A at 7 days (H) in CFC test after chemogenetic activation of SuM-enhanced ABNs. For WT mice, n = 10 mice for each group; for AD mice, n = 6 mice for mCherry group, and n = 8 mice for ChR2 group.
(I–L) Affective behavior tests following chemogenetic activation of SuM-enhanced ABNs. For WT mice, n = 10 mice for each group; for AD mice, n = 6 mice for mCherry group, and n = 8 mice for ChR2 group.
Data are represented as mean ± SEM. *$p < 0.05$, **$p < 0.01$ by two-way ANOVA, followed by Tukey's post hoc test.

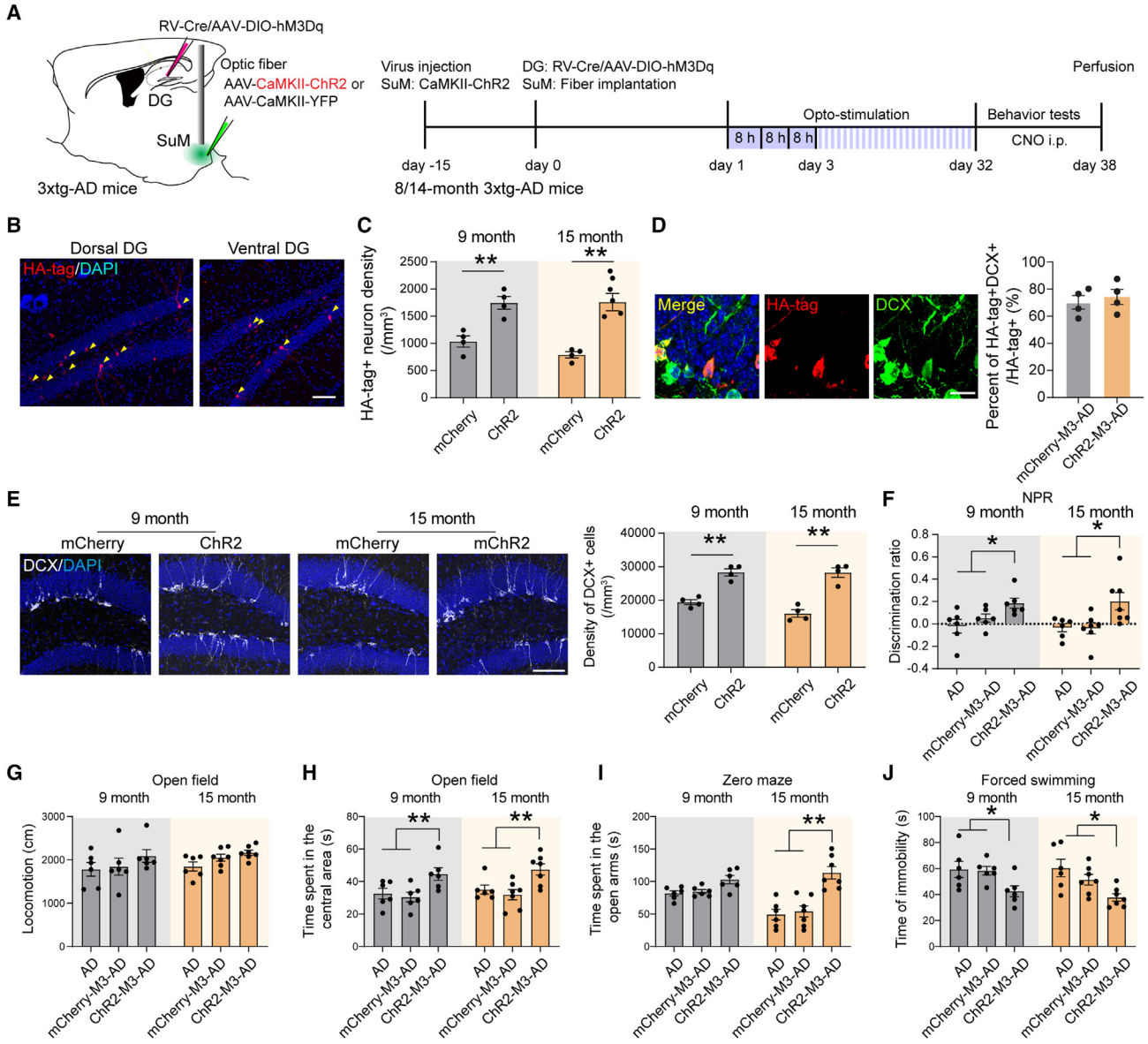

Figure 4. Acute chemogenetic activation of SuM-enhanced ABNs rescues cognitive and affective deficits in aged 3×Tg-AD mice

(A) Experimental scheme. AAV-CaMKII-ChR2-YFP or AAV-CaMKII-YFP was injected into SuM. After 2 weeks, retrovirus (RV)-Cre-HA and AAV-DIO-hM3Dq-mCherry was co-injected into both dorsal and ventral DGs, with fiber implantation above SuM. 1 day after optogenetic stimulation of SuM, behaviors were tested with CNO injection to activated ABNs.

(B) Images of HA staining indicated ABNs with hM3Dq expression in dorsal and ventral DG. Scale bars, 100 μm.

(C) Chronic stimulation of SuM increased HA+ ABNs in both 9-month-old and 15-month-old 3×Tg-AD mice. n = 4 mice for each group.

(D) Expression of DCX in HA+ cells. Scale bars, 20 μm. n = 4 mice for each group.

(E) Chronic stimulation of SuM increased total DCX+ cells. n = 4 mice for each group. Scale bars, 100 μm.

(F) Chemogenetic activation of SuM-enhanced ABNs promoted spatial memory retrieval in the NPR test.

(G and H) Chemogenetic activation of SuM-enhanced ABNs did not alter locomotion (G), but increased time spent in the center area (H) in the open field test.

(I) Chemogenetic activation of SuM-enhanced ABNs increased time spent in the open arms in the zero maze test in the 15-month-old 3×Tg-AD mice.

(J) Chemogenetic activation of SuM-enhanced ABNs decreased time of immobility in the forced swimming test. n = 6–7 mice for each group.

Data are represented as mean ± SEM. *$p < 0.05$, **$p < 0.01$ by unpaired t test or two-way ANOVA, followed by Tukey's post hoc test.

in 5×FAD mice. To probe activity-dependent signaling mechanisms mediated by SuM-enhanced ABNs, we performed phosphoproteomics of the whole hippocampus from 4.5-month-old ChR2-AM3-AD and mCherry-AM3-AD mice following acute chemogenetic activation of SuM-enhanced and control ABNs using label-free quantitative (LFQ) method coupled with liquid chromatography-tandem mass spectrometry (LC-MS/MS).[39] Brain tissues were collected 30–60 min after intraperitoneal injection of

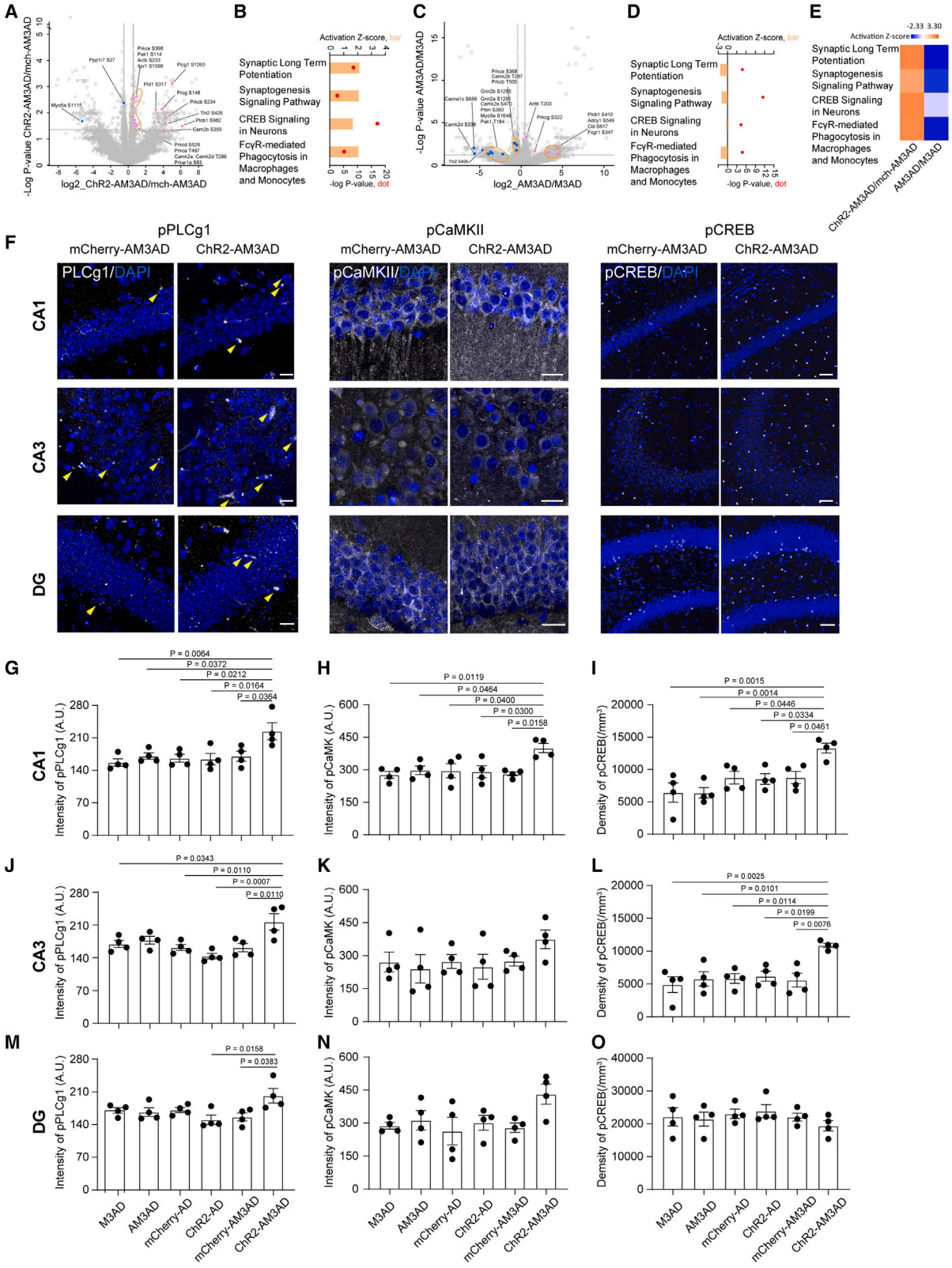

(legend on next page)

CNO to match the timing of the behavioral tests (Figure 3A). Phosphoproteomics analyses identified 21,894 phosphorylation sites from 4,121 phosphoproteins, and the changes of 13,643 phosphorylation sites were quantified (Table S1). Among them, 717 sites from 540 proteins showed altered levels of phosphorylation with p values $\leq$ 0.05 and $\log_2$ ratios ≤ -0.50 or $\geq$ 0.50 when comparing SuM-stimulated ChR2-AM3-AD to sham control mCherry-AM3-AD mice following CNO administration (Figure 5A), without significantly altering the global protein level (Figures S6A and S6B). Interestingly, gene ontology analyses of pathways showed that the majority of canonical signaling pathways (64 out of 72) exhibited activation upon acute stimulation of SuM-enhanced ABNs (Figure S6C; Table S2). Among these pathways, we found significant activation in pathways related to synaptic plasticity, such as long-term potentiation (LTP), CREB signaling, and synaptogenesis (Figures 5B, 5E, and S6C). Some phosphoproteins within these pathways have been widely implicated in learning and memory, including CaMKII (CaMKIIA and CaMKIIB) and PLCg1.[40–42] Interestingly, we also found significant activation in pathways related to microglia phagocytosis of plaques, such as FCγ receptor-mediated phagocytosis in microglia[43] (Figures 5A and 5B). Some phosphorylated proteins in this pathway have been implicated in plaque clearance, such as PAK1[44] (Figures 5A and 5B).

As a negative control, we performed similar phosphoproteomics analyses of the hippocampus from AM3-AD and M3-AD mice following acute chemogenetic activation of control ABNs (without SuM modification), as ABN activation in AM3-AD mice did not improve behaviors. Brain tissues were collected 30–60 min after intraperitoneal injection of CNO to match the behavioral readouts (Figure 3A). As a result, 830 differentially phosphorylated sites from 633 phosphoproteins were identified following acute ABN activation (Figure 5C; Table S1). Interestingly, in contrast to predominantly activated canonical pathways in ChR2-AM3-AD/mCherry-AM3-AD mice (Figure S7), most canonical pathways (39 out of 50) were suppressed when comparing AM3-AD to M3-AD mice (Figures 5D, 5E, and S6D; Table S3), including the ones related to synaptic plasticity and microglial phagocytosis of plaques (Figures 5D, 5E, and S6D). Together, these results revealed activity-dependent signaling mechanisms that may underlie distinct behavioral readouts mediated by activation of SuM-enhanced vs. control ABNs in AD brains.

Activation of SuM-enhanced ABNs induces hippocampal-subregion-specific alteration of phosphoproteins related to synaptic plasticity in 5× FAD mice

Converging evidence suggests that ABNs can modulate DG and CA3 dynamics through direct synaptic contacts with DG/hilar and CA3 interneurons (INs) and principle cells.[15,45–48] Furthermore, ABNs can indirectly modulate CA1 through ABN-CA3-CA1 connections. Therefore, activation of SuM-enhanced ABNs may exert distinct effects on the activity dynamics and synaptic plasticity of different hippocampal subfields. Given that our phosphoproteomics was performed using tissues from the whole hippocampus, we intended to validate some of the key differentially regulated phosphoproteins (DRPs) using immunohistochemistry following acute chemogenetic activation of SuM-enhanced or control ABNs in SuM or sham stimulated ChR2/mCherry-AM3-AD mice to obtain hippocampal-subregion-specific information on their expression. We also included hippocampal tissues from the 5×FAD mice with SuM-stimulation only (mCherry-AD vs. ChR2-AD) and acute chemogenetic activation of ABNs without SuM modification (M3-AD vs. AM3-AD) as additional controls. Several key DRPs involved in synaptic plasticity, including pPLCg1, pCaMKII, and pCREB, were selected for validation (Figure 5F). Interestingly, these DRPs exhibit distinct expression patterns in different hippocampal subfields (DG, CA3, and CA1) following acute activation of SuM-enhanced ABNs. Specifically, acute chemogenetic activation of SuM-enhanced (vs. control) ABNs induced significantly increased expression of pPLCg1, pCaMKII, and pCREB in CA1 (Figures 5G–5I), pPLCg1 and pCREB in CA3 (Figures 5J–5L), and pPLCg1 in DG (Figures 5M–5O), as compared with various controls. These results provided hippocampal subregion-specific signaling mechanisms mediated by activation of SuM-enhanced ABNs.

Activation of SuM-enhanced ABNs increases CA1 LTP in 5×FAD mice

Given that CA1 among all hippocampal subfields exhibited the broad alteration of selected DRPs, we decided to perform functional validation of synaptic plasticity in CA1 by recording LTP upon acute chemogenetic activation of SuM-enhanced ABNs in acute brain slices prepared from SuM or sham stimulated ChR2/mCherry-AM3-AD mice (Figure 6A). Additional controls

Figure 5. Acute chemogenetic activation of SuM-enhanced ABNs induces hippocampal-subregion-specific alteration of phosphoproteins in 5×FAD mice

(A) Quantitative phosphoproteomic analyses (whole hippocampal tissues) comparing SuM-stimulated ChR2-AM3AD and sham control mCherry-AM3AD mice following CNO administration. Label-free quantitation was performed with a p value of 0.05 and $\log_2$ ratios of ±0.50 to report statistically significant up-regulated or down-regulated phosphorylated sites. Three mice for each group and 2 LC-MS/MS technical replicates of enriched phosphorylated peptides were generated from each mouse.

(B) Selected activated canonical signaling pathways comparing ChR2-AM3AD to mCherry-AM3AD mice. Cutoff: *Z* score ±1.0, p value < 0.05, same in (D).

(C) Quantitative phosphoproteomic analyses comparing AM3AD and M3AD mice following CNO administration.

(D) Selected canonical signaling pathways comparing AM3AD to M3AD mice.

(E) A heatmap of the *Z* scored canonical signaling pathways, ChR2-AM3AD vs. mCherry-AM3AD, and AM3AD vs. M3AD mice.

(F) Representative images of pPLCg1, pCaMKII, and pCREB immunofluorescence staining in CA1, CA3, and DG from mCherry-AM3AD and ChR2-AM3AD mice. Scale bars, 20 μm.

(G–O) Quantification of fluorescence density of pPLCg1, pCaMKII, and density of pCREB in CA1 (G–I), CA3 (J–L), and DG (M–O) from 4.5-month-old M3AD, AM3AD, mCherry-AD, ChR2-AD, mCherry-AM3AD-, and ChR2-AM3AD mice, respectively. n = 4 mice for each group.

Data are represented as mean ± SEM. Comparisons were using one-way ANOVA, followed by Tukey's post hoc test.

See also Figures S6 and S7 and Tables S1, S2, and S3.

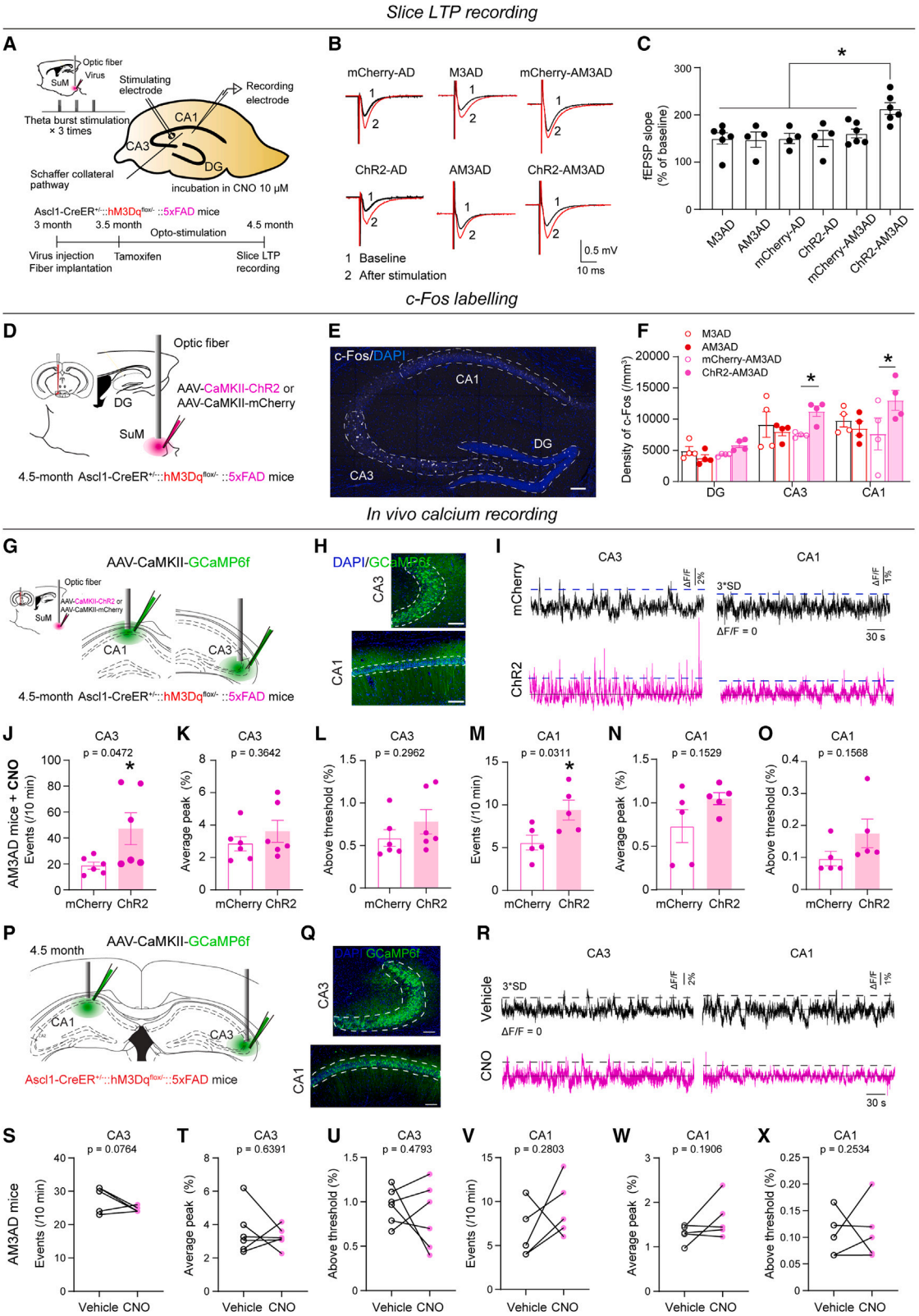

(legend on next page)

from the 5×FAD mice with SuM-stimulation only (mCherry-AD vs. ChR2-AD), and acute chemogenetic activation of ABNs without SuM modification (M3-AD vs. AM3-AD), were also included for cross comparison. Interestingly, acute chemogenetic activation of ABNs in ChR2-AM3-AD mice through bath application of CNO led to a significant increase in CA1 LTP, as compared with various controls (Figures 6B and 6C). Together with phosphoprotein data (Figures 5A–5E), these results demonstrated that activation of SuM-enhanced ABNs increases hippocampal CA1 LTP along with increased expression of phosphoproteins involved in synaptic plasticity, including pPLCg1, pCaMKII, and pCREB.

Activation of SuM-enhanced ABNs increases CA3 and CA1 activity in 5×FAD mice

CREB signaling is highly implicated in neuronal activity and learning/memory.[49,50] Therefore, activation of CREB signaling in neurons promoted us to ask whether activation of SuM-enhanced ABNs alters local hippocampal circuit activity. We first examined c-Fos expression in DG, CA3, and CA1 following acute chemogenetic activation of SuM-enhanced vs. control ABNs in 4.5-month-old ChR2-AM3-AD or mCherry-AM3-AD mice, respectively (Figure 6D). Interestingly, activation of SuM-enhanced (vs. control) ABNs increased c-Fos expression in CA3 and CA1, but not DG (Figures 6E and 6F). To confirm the c-Fos results, we performed fiber photometry to record calcium activity of CA3 and CA1 pyramidal neurons labeled with GCaMP6f upon chemogenetic activation of SuM-enhanced ABNs by intraperitoneal CNO injection (Figures 6G and 6H). Compared to mCherry-AM3-AD control mice, activation of SuM-enhanced ABNs in ChR2-AM3-AD mice increased the frequency of calcium events in both CA1 and CA3 without altering the amplitude of these events (Figures 6I–6O). By contrast, activation of control ABNs without SuM modification in AM3-AD mice failed to alter c-Fos expression and calcium activity in CA3 and CA1 (Figures 6F and 6P–6X). These results suggested that activation of SuM-enhanced ABNs increased hippocampal CA3 and CA1 (but not DG) activity, which aligns with the phosphoproteomics data showing increased expression of pCREB only in CA3 and CA1 (but not DG).

Activation of SuM-enhanced ABNs increases microglial phagocytosis of plaques in 5×FAD mice

Our quantitative phosphoproteomics of the hippocampus in 5×FAD mice showed that acute chemogenetic activation of SuM-enhanced (vs. control) ABNs activates the pathways for Fcγ receptor-mediated microglia phagocytosis, while chemogenetic activation of ABNs without SuM modification in 5×FAD mice suppressed this pathway (Figure 5E). These data support the interaction between activity of SuM-enhanced ABNs and microglia dynamics. Supporting this view, we found that tdToamto+ ABN mossy fibers are closely associated with Iba+ microglia in the DG/hilus where the most severe plaque deposition was observed among all hippocampal subfields in Ascl1-Ai9-AD mice (Figures 7A and 7B). We then examined microglia phagocytosis of plaques following acute chemogenetic activation of SuM-enhanced or control ABNs in ChR2/mCherry AM3-AD mice by Imaris imaging analysis. Interestingly, acute activation of SuM-enhanced (vs. control) ABNs increased microglial engulfment of Thio-S+ plaques (Figures 7C and 7D) without altering the volumes of Iba1+ fluorescence and Thio-S (Figures 7E and 7F). By contrast, acute activation of ABNs without SuM modification in AD mice failed to alter microglial engulfment of Thio-S+ plaques (Figures 7G–7I).

Furthermore, we analyzed non-plaque-associated microglia morphology after acute chemogenetic activation of SuM-enhanced or control ABNs in ChR2-AM3-AD or mCherry-AM3-AD mice, respectively. Additional controls were included for cross comparison, including the 5×FAD mice with SuM-stimulation only (mCherry-AD vs. ChR2-AD) and acute chemogenetic activation of ABNs without SuM modification (M3-AD vs. AM3-AD), as well as WT mice. The density of the microglia was not

Figure 6. Acute chemogenetic activation of SuM-enhanced ABNs modulates hippocampal circuit activity dynamics and synaptic plasticity in 5×FAD mice

(A) Diagram of slice LTP recording in CA1. Schematic diagram described the location of the stimulus electrode and recording electrode in the dorsal hippocampal slices. CNO 10 μM was bath applied constantly throughout the entire recording.
(B) Traces of fEPSPs before (1) and after (2) induction of LTP from an M3AD, AM3AD, mCherry-AD, ChR2-AD, mCherry-AM3AD, and ChR2-AM3AD mouse, respectively.
(C) Bar graphs show mean values of fEPSP slope changes (%) measured 50–60 min after TBS from 4.5-month-old M3AD, AM3AD, mCherry-AD, ChR2-AD, mCherry-AM3AD, and ChR2-AM3AD mice, respectively. n = 4–6 slices from 4 to 5 mice for each group.
(D) Experimental scheme for c-Fos quantification.
(E) Representative image of c-Fos expression in the hippocampus. Scale bars, 200 μm.
(F) Density of c-Fos in the DG, CA3, and CA1. n = 4 mice for each group.
(G) Fiber photometry recording of CA1 and CA3 pyramidal neurons following activation of SuM-enhanced ABNs.
(H) Representative confocal images of GCaMP expression in CA3 and CA1 pyramidal neurons. Scale bars, 100 μm.
(I) Representative traces of population calcium activity in CA1 and CA3 pyramidal neurons 30 min after CNO 0.5 mg/kg i.p. injection.
(J–L) Events (J), average peak (K), and percent above thresholds (L) of population calcium activity in CA3 pyramidal neurons. n = 6 mice in each group.
(M–O) Events (M), average peak (N), and percent above thresholds (O) of population calcium activity in CA1 pyramidal neurons. n = 5 mice in each group.
(P) Experimental scheme for fiber photometry recording of CA1 and CA3 pyramidal neurons.
(Q) Representative images of GCaMP expression in CA1 and CA3 pyramidal neurons. Scale bars, 100 μm.
(R) Representative traces of population calcium activity in CA1 and CA3 pyramidal neurons 30 min after vehicle or CNO 0.5 mg/kg i.p. injection.
(S–U) Events (S), average peak (T), and percent above thresholds (U) of population calcium activity in CA3 pyramidal neurons in AM3AD mice after vehicle or CNO injection. n = 6 mice in each group.
(V–X) Events (V), average peak (W), and percent above thresholds (X) of population calcium activity in CA1 pyramidal neurons in AM3AD mice after vehicle or CNO injection. n = 5 mice in each group.
Data are represented as mean ± SEM. *$p < 0.05$ by unpaired or paired t test, or one-way ANOVA, followed by Tukey's post hoc test.

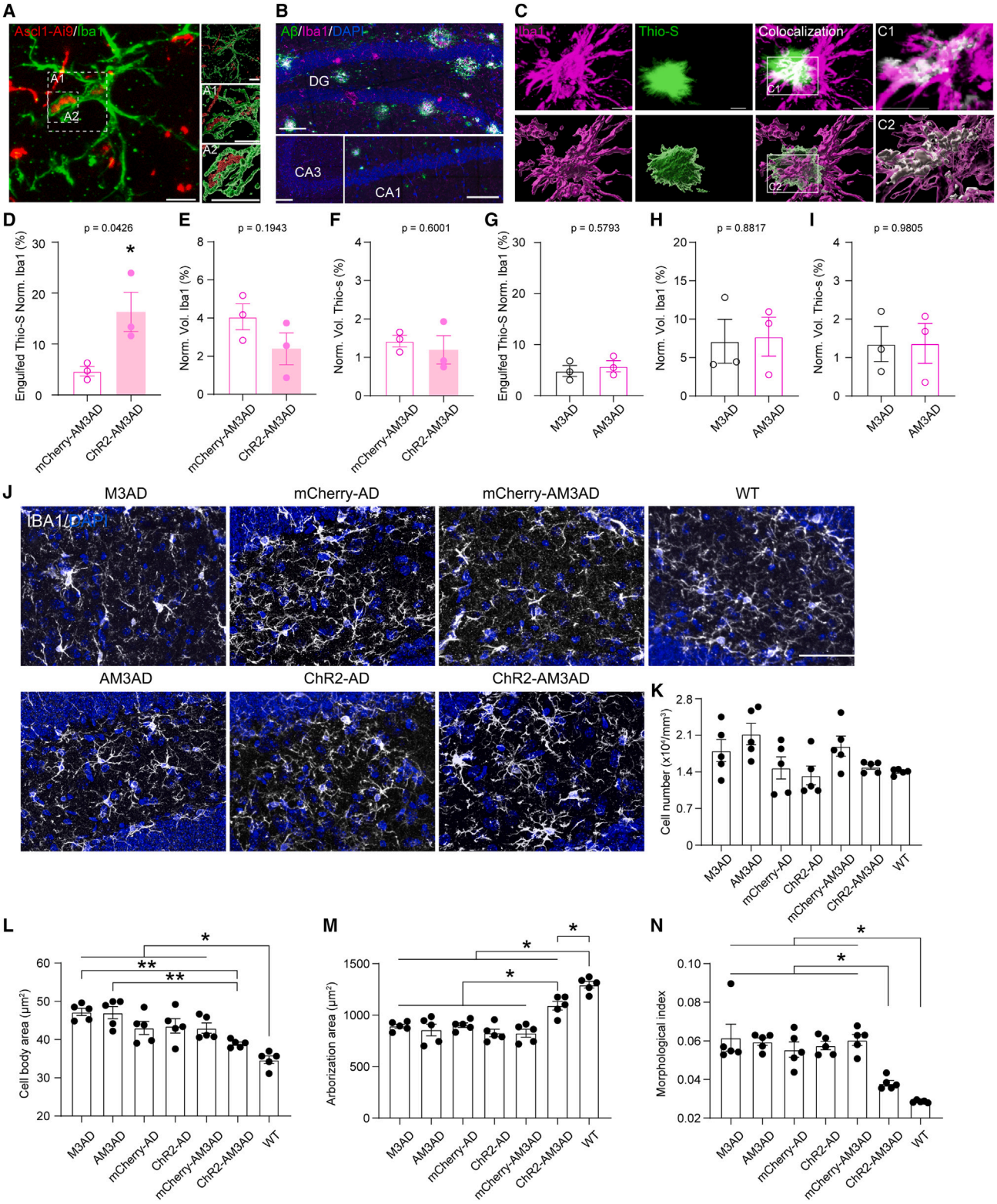

Figure 7. Acute chemogenetic activation of SuM-enhanced ABNs improves microglial properties in 5×FAD mice

(A) Representative images and 3D reconstruction of Ascl1+ ABN mossy fibers and microglia in the hilus. (A1 and A2) 3D reconstruction of tdTomato and IBA1 staining fluorescence. Scale bars, 5 μm.

(B) Representative confocal images of Aβ and Iba1 staining in the DG, CA3, and CA1 in 4.5-month-old AD mice. Scale bars, 100 μm.

(legend continued on next page)

altered across multiple experimental and control groups (Figures 7J and 7K). It has been reported that microglia in AD mice exhibit enlarged soma and retracted processes, which represent a pathological state.[51,52] Consistent with these findings, we found similar morphological features of microglia in the DG of 5×FAD mice, characterized by an increased soma area (Figure 7L), reduced arborization of processes (Figure 7M), and an increased morphological index (Figure 7N), as compared with WT mice. Strikingly, acute activation of SuM-enhanced ABNs significantly decreased the soma area, increased arborization of processes, and decreased the morphological index of microglia (Figures 7L–7N), as compared with various control groups mentioned above. These results suggested that the activation of SuM-enhanced ABNs promotes microglial phagocytosis of plaques and improves microglial morphology in AD mice.

DISCUSSION

Substantial studies by immunohistology and single-nucleus RNA sequencing using human postmortem tissues have revealed impaired AHN in various neurological and psychiatric disorders, including AD,[6–9] Lewy body dementia,[53] and major depressive disorders.[54] Therefore, targeting AHN may represent a new avenue to restore cognitive and affective function in diseased brains. Because AHN is impaired in AD patients, a long-standing question has centered on whether modulating AHN alone is sufficient to rescue cognitive and affective deficits in AD. Our study showed that acute chemogenetic activation of ABNs without SuM modulation fails to rescue hippocampal deficits in 5×FAD mice (Figure S8A), suggesting that stimulating the activity of impaired ABNs in AD brains is not beneficial for hippocampal function. In addition, although chronic patterned opto-stimulation of SuM restored AHN in AD mice, it failed to restore hippocampal function or alter major AD pathology (Figure S8B). By contrast, the combination of opto-stimulation of SuM with subsequent chemogenetic activation of SuM-enhanced ABNs can reverse hippocampal deficits in AD mice (Figure S8C). Therefore, our study highlights activity-dependent contribution of SuM-enhanced ABNs to hippocampal function in AD brains.

Besides the effects on hippocampal activity and plasticity, acute activation of SuM-enhanced ABNs also increases microglia phagocytosis of plaques (plaque-associated microglia) and improves microglial morphology (non-plaque-associated microglia) in 5×FAD mice. Due to the acute nature of activity manipulation of these ABNs, we do not expect that acute modulation of microglial properties contributes to the improved hippocampal function observed in 5×FAD mice. However, it is possible that chronic stimulation of SuM-enhanced ABNs may benefit hippocampal function in AD through improved microglial function by reducing plaques and correcting aberrant synaptic pruning. Future studies that test various aspects of hippocampal function following chronic activation of SuM-enhanced ABNs during the critical window will be able to address this question.

ABNs can modulate DG and CA3 activity dynamics and synaptic plasticity by forming direct synaptic connections with DG/hilar and CA3 INs, DG granule cells (GCs), and CA3 pyramidal cells (PCs). Therefore, ABNs can form disynaptic inhibitory inputs and monosynaptic excitatory inputs onto DG GCs and CA3 PCs.[15,45–48] These concurrent excitatory and inhibitory inputs collectively contribute to feedback/feedforward inhibition, along with feedback/feedforward excitation onto DG GCs and CA3 PCs. Furthermore, ABNs can also modulate CA1 activity dynamics and synaptic plasticity indirectly through ABN-CA3-CA1 connections. How activation of SuM-enhanced ABNs modulates hippocampal circuit dynamics of AD mice remains unknown. Our phosphoproteomics analyses along with functional assays provide hippocampal-subregion-specific signaling mechanisms underlying ABN-activity-dependent modulation of hippocampal circuit dynamics (Figure S8D). Specifically, acute chemogenetic activation of SuM-enhanced (vs. control) ABNs increased activity in CA3 and CA1 (but not DG) of AD mice. These results support the view that activation of SuM-enhanced ABNs exerts a net excitation on CA3 potentially through dominant feedforward excitation from ABNs to CA3 PCs over feedforward inhibition from ABNs-CA3 INs-CA3 PCs, which in turns activates CA1 PCs. Interestingly, acute activation of SuM-enhanced ABNs did not impact activity of DG GCs, potentially due to concurrent feedback inhibition and excitation onto GCs, thus leading to unaltered overall activity. These region-specific activity changes perfectly match the expression pattern of pCREB in these distinct hippocampal subfields, thus revealing pCREB as a neuronal signaling molecule highly responsive to activation of SuM-enhanced ABNs. In contrast to pCREB showing hippocampal-subregion-specific expression, pPLCg1 exhibited increased expression in all hippocampal subfields, including DG, CA3, and CA1. pPLCg1 is highly implicated in LTP, so these results suggest that activation of SuM-enhanced ABNs may enhance LTP in all hippocampal subregions (note: only CA1 LTP is validated in the current study).

Our study showed that activation of ABNs without SuM modulation in AD mice fails to improve hippocampal function. These results highlight the critical role of SuM modulation of ABNs in mediating activity-dependent benefits in hippocampal function. SuM is a small brain structure located within the hypothalamus, and recent studies have shown that SuM is critical for the hippocampal theta rhythm,[55–57] sleep-wake cycles,[58] behavioral

(C) Sample images showing Aβ plaque (thio-S+) and microglia (Iba1+) for co-localization analysis. Top: confocal images. Bottom: 3D reconstruction by Imaris. Scale bars, 5 μm.
(D) Normalized engulfed of Iba1 and Thio-S in the DG of 4.5-month-old mCherry-AM3AD and ChR2-AM3AD mice. n = 3 mice in each group.
(E and F) Normalized volume of Iba1 (E) and Thio-S (F) in the DG of 4.5-month-old mCherry-AM3AD and ChR2-AM3AD mice. n = 3 mice in each group.
(G) Normalized engulfed of Iba1 and Thio-S in the DG of 4.5-month-old M3AD and AM3AD mice. n = 3 mice in each group.
(H and I) Normalized volume of Iba1 (H) and Thio-S (I) in the DG in 4.5-month-old M3AD and AM3AD mice. n = 3 mice in each group.
(J) Representative images of Iba1 staining in the DG in 4.5-month-old AD mice following activation of control ABNs (M3AD/AM3AD), chronic SuM stimulation (mCherry-AD/ChR2-AD), and chemogenetic activation of SuM-enhanced ABNs (mCherry-AM3AD/ChR2-AM3AD). Scale bars, 100 μm.
(K) Quantification of the density of Iba1+ cells in the DG.
(L–N) Quantification of microglia cell body area (L), arborization area (M), and morphological index (N). n = 5 mice in each group.
Data are represented as mean ± SEM. *$p < 0.05$, **$p < 0.01$ by unpaired t test or one-way ANOVA, followed by Tukey's post hoc test.

responses to novelty signals,[59,60] and locomotion.[61] Importantly, this brain structure is largely spared from plaque deposition during disease progression,[62] thus avoiding the potential release of toxic chemicals upon stimulation. In addition, SuM forms direct inputs to NSCs and ABNs,[22] thus ensuring its beneficial effects on AHN despite being in a neurogenic niche with AD pathology. These features make it an ideal candidate for therapeutic intervention, potentially through deep brain stimulation.

In summary, our findings present the evidence that boosting the activity of a small population of ABNs with enhanced properties is sufficient to restore cognitive and affective deficits associated with AD. Importantly, our studies provide novel ABN-activity-dependent signaling mechanisms underlying the functional improvement in AD brains mediated by the activation of SuM-enhanced ABNs. Recently, the existence of adult human hippocampal neurogenesis has gained increasing support.[6–12] It is generally agreed that low-level neurogenesis exists in adult humans across aging, potentially via low-frequency *de novo* generation of ABNs from adult NSPCs and protracted maturation of ABNs.[9] In AD brains, this level is even lower.[6–9] By manipulating a small population of ABNs, our findings provide timely answers to the long-standing question of how to effectively enhance ABNs to restore hippocampal function in degenerated AD brains.[18]

Limitations of the study

There are some limitations in this study. First, we used two AD mouse models, 5×FAD and 3×Tg-AD, which carry different transgenes and exhibit different disease progression patterns. However, they both overexpress the disease genes. Therefore, they do not fully recapitulate human AD pathologies. In future, we will consider knockin mouse models of AD to extend our findings to a more physiological context for AD pathologies. Second, we focused on validation of the phosphoproteins related to synaptic plasticity because neuronal populations are enriched in bulk hippocampal tissues used for our phosphoproteomics analyses. The phosphoproteins related to microglial phagocytosis remain to be validated. Third, the behavioral data presented in Figure 4 were only collected from AD animals (3×Tg-AD) as a validation for the data from 5×FAD mice. Therefore, direct cross comparison of AD and WT data was not immediately available.

STAR★METHODS

Detailed methods are provided in the online version of this paper and include the following:

- KEY RESOURCES TABLE
- RESOURCE AVAILABILITY
  - Lead contact
  - Materials availability
  - Data and code availability
- EXPERIMENTAL MODEL AND SUBJECT DETAILS
  - Experimental animals
  - Choice of the mouse model
- METHOD DETAILS
  - Stereotaxic surgery
  - Fiber photometry recording and analysis
  - Chemical administration and optogenetic/chemogenetic stimulation protocol
  - Immunohistochemistry (IHC)
  - Image analysis
  - Behavioral tests
  - Long-term potentiation (LTP) recording
- QUANTIFICATION AND STATISTICAL ANALYSIS

SUPPLEMENTAL INFORMATION

Supplemental information can be found online at https://doi.org/10.1016/j.stem.2023.02.006.

ACKNOWLEDGMENTS

We thank all the members of the Song lab for comments and discussions. We also thank Dr. Bryan Roth for proving floxed hM3Dq mice. This work was supported by grants awarded to J.S. from NIH (R01MH111773, R01MH122692, RF1AG058160, and R01NS104530) and Alzheimer's Association and to X.C. from NIH (R21AG071229, R01GM133107). Y.-D.L. was partially supported by a NARSAD Young Investigator grant from the Brain & Behavior Research Foundation (29600). R.N.S. is supported by UNC Pharmacology Curriculum predoctoral T32 training grant. Confocal microscopy was performed at the UNC Neuroscience Microscopy Core Facility (RRID: SCR_019060) with technical assistance from Dr. Michelle S. Itano. The Neuroscience Microscopy Core was supported in part by funding from the NIH-NINDS Neuroscience Center Support grant P30 NS045892 and the NIH-NICHD Intellectual and Developmental Disabilities Research Center Support grant U54 HD079124.

AUTHOR CONTRIBUTIONS

J.S. conceived and supervised the project, designed the experiments, and wrote the paper. Y.-D.L. designed the experiments, wrote the paper, and carried out experiments and data analysis. Y.-J.L. carried out all aspects of electrophysiology experiments and data analysis and assisted in preparing the manuscript. L.X. and X.C. performed phosphoproteomics analyses and helped with manuscript preparation. D.S.T. and R.N.S. performed microglia phagocytosis analysis. L.Z. provided technical supports for the project. L.G.C. provided aged 3×Tg-AD mice.

DECLARATION OF INTERESTS

The authors declare no competing interests.

Received: September 6, 2022
Revised: December 29, 2022
Accepted: February 14, 2023
Published: April 6, 2023

REFERENCES

1. Selkoe, D.J. (2001). Alzheimer's disease: genes, proteins, and therapy. Physiol. Rev. *81*, 741–766. https://doi.org/10.1152/physrev.2001.81.2.741.
2. Selkoe, D.J. (2002). Alzheimer's disease is a synaptic failure. Science *298*, 789–791. https://doi.org/10.1126/science.1074069.
3. Palmer, K., Berger, A.K., Monastero, R., Winblad, B., Bäckman, L., and Fratiglioni, L. (2007). Predictors of progression from mild cognitive impairment to Alzheimer disease. Neurology *68*, 1596–1602. https://doi.org/10.1212/01.wnl.0000260968.92345.3f.
4. Ehrenberg, A.J., Suemoto, C.K., França Resende, E.P., Petersen, C., Leite, R.E.P., Rodriguez, R.D., Ferretti-Rebustini, R.E.L., You, M., Oh, J., Nitrini, R., et al. (2018). Neuropathologic correlates of psychiatric symptoms in Alzheimer's disease. J. Alzheimers. Dis. *66*, 115–126. https://doi.org/10.3233/JAD-180688.

5. Phelps, E.A. (2004). Human emotion and memory: interactions of the amygdala and hippocampal complex. Curr. Opin. Neurobiol. *14*, 198–202. https://doi.org/10.1016/j.conb.2004.03.015.
6. Moreno-Jiménez, E.P., Flor-García, M., Terreros-Roncal, J., Rábano, A., Cafini, F., Pallas-Bazarra, N., Ávila, J., and Llorens-Martín, M. (2019). Adult hippocampal neurogenesis is abundant in neurologically healthy subjects and drops sharply in patients with Alzheimer's disease. Nat. Med. *25*, 554–560. https://doi.org/10.1038/s41591-019-0375-9.
7. Tobin, M.K., Musaraca, K., Disouky, A., Shetti, A., Bheri, A., Honer, W.G., Kim, N., Dawe, R.J., Bennett, D.A., Arfanakis, K., and Lazarov, O. (2019). Human hippocampal neurogenesis persists in aged adults and Alzheimer's disease patients. Cell Stem Cell *24*, 974–982.e3. https://doi.org/10.1016/j.stem.2019.05.003.
8. Terreros-Roncal, J., Moreno-Jiménez, E.P., Flor-García, M., Rodríguez-Moreno, C.B., Trinchero, M.F., Cafini, F., Rábano, A., and Llorens-Martín, M. (2021). Impact of neurodegenerative diseases on human adult hippocampal neurogenesis. Science *374*, 1106–1113. https://doi.org/10.1126/science.abl5163.
9. Zhou, Y., Su, Y., Li, S., Kennedy, B.C., Zhang, D.Y., Bond, A.M., Sun, Y., Jacob, F., Lu, L., Hu, P., et al. (2022). Molecular landscapes of human hippocampal immature neurons across lifespan. Nature *607*, 527–533. https://doi.org/10.1038/s41586-022-04912-w.
10. Ammothumkandy, A., Ravina, K., Wolseley, V., Tartt, A.N., Yu, P.N., Corona, L., Zhang, N., Nune, G., Kalayjian, L., Mann, J.J., et al. (2022). Altered adult neurogenesis and gliogenesis in patients with mesial temporal lobe epilepsy. Nat. Neurosci. *25*, 493–503. https://doi.org/10.1038/s41593-022-01044-2.
11. Spalding, K.L., Bergmann, O., Alkass, K., Bernard, S., Salehpour, M., Huttner, H.B., Boström, E., Westerlund, I., Vial, C., Buchholz, B.A., et al. (2013). Dynamics of hippocampal neurogenesis in adult humans. Cell *153*, 1219–1227. https://doi.org/10.1016/j.cell.2013.05.002.
12. Wang, W., Wang, M., Yang, M., Zeng, B., Qiu, W., Ma, Q., Jing, X., Zhang, Q., Wang, B., Yin, C., et al. (2022). Transcriptome dynamics of hippocampal neurogenesis in macaques across the lifespan and aged humans. Cell Res. *32*, 729–743. https://doi.org/10.1038/s41422-022-00678-y.
13. Clelland, C.D., Choi, M., Romberg, C., Clemenson, G.D., Jr., Fragniere, A., Tyers, P., Jessberger, S., Saksida, L.M., Barker, R.A., Gage, F.H., and Bussey, T.J. (2009). A functional role for adult hippocampal neurogenesis in spatial pattern separation. Science *325*, 210–213. https://doi.org/10.1126/science.1173215.
14. Sahay, A., Scobie, K.N., Hill, A.S., O'Carroll, C.M., Kheirbek, M.A., Burghardt, N.S., Fenton, A.A., Dranovsky, A., and Hen, R. (2011). Increasing adult hippocampal neurogenesis is sufficient to improve pattern separation. Nature *472*, 466–470. https://doi.org/10.1038/nature09817.
15. Gu, Y., Arruda-Carvalho, M., Wang, J., Janoschka, S.R., Josselyn, S.A., Frankland, P.W., and Ge, S. (2012). Optical controlling reveals time-dependent roles for adult-born dentate granule cells. Nat. Neurosci. *15*, 1700–1706. https://doi.org/10.1038/nn.3260.
16. Danielson, N.B., Kaifosh, P., Zaremba, J.D., Lovett-Barron, M., Tsai, J., Denny, C.A., Balough, E.M., Goldberg, A.R., Drew, L.J., Hen, R., et al. (2016). Distinct contribution of adult-born hippocampal granule cells to context encoding. Neuron *90*, 101–112. https://doi.org/10.1016/j.neuron.2016.02.019.
17. McHugh, S.B., Lopes-Dos-Santos, V., Gava, G.P., Hartwich, K., Tam, S.K.E., Bannerman, D.M., and Dupret, D. (2022). Adult-born dentate granule cells promote hippocampal population sparsity. Nat. Neurosci. *25*, 1481–1491. https://doi.org/10.1038/s41593-022-01176-5.
18. Li, Y.D., Luo, Y.J., and Song, J. (2023). Optimizing memory performance and emotional states: multi-level enhancement of adult hippocampal neurogenesis. Curr. Opin. Neurobiol. *79*, 102693. https://doi.org/10.1016/j.conb.2023.102693.
19. Snyder, J.S., Soumier, A., Brewer, M., Pickel, J., and Cameron, H.A. (2011). Adult hippocampal neurogenesis buffers stress responses and depressive behaviour. Nature *476*, 458–461. https://doi.org/10.1038/nature10287.
20. Anacker, C., Luna, V.M., Stevens, G.S., Millette, A., Shores, R., Jimenez, J.C., Chen, B., and Hen, R. (2018). Hippocampal neurogenesis confers stress resilience by inhibiting the ventral dentate gyrus. Nature *559*, 98–102. https://doi.org/10.1038/s41586-018-0262-4.
21. Kempermann, G., Kuhn, H.G., and Gage, F.H. (1997). More hippocampal neurons in adult mice living in an enriched environment. Nature *386*, 493–495. https://doi.org/10.1038/386493a0.
22. Li, Y.D., Luo, Y.J., Chen, Z.K., Quintanilla, L., Cherasse, Y., Zhang, L., Lazarus, M., Huang, Z.L., and Song, J. (2022). Hypothalamic modulation of adult hippocampal neurogenesis in mice confers activity-dependent regulation of memory and anxiety-like behavior. Nat. Neurosci. *25*, 630–645. https://doi.org/10.1038/s41593-022-01065-x.
23. van Praag, H., Kempermann, G., and Gage, F.H. (1999). Running increases cell proliferation and neurogenesis in the adult mouse dentate gyrus. Nat. Neurosci. *2*, 266–270.
24. Choi, S.H., Bylykbashi, E., Chatila, Z.K., Lee, S.W., Pulli, B., Clemenson, G.D., Kim, E., Rompala, A., Oram, M.K., Asselin, C., et al. (2018). Combined adult neurogenesis and BDNF mimic exercise effects on cognition in an Alzheimer's mouse model. Science *361*, eaan8821. https://doi.org/10.1126/science.aan8821.
25. Walgrave, H., Balusu, S., Snoeck, S., Vanden Eynden, E., Craessaerts, K., Thrupp, N., Wolfs, L., Horré, K., Fourne, Y., Ronisz, A., et al. (2021). Restoring miR-132 expression rescues adult hippocampal neurogenesis and memory deficits in Alzheimer's disease. Cell Stem Cell *28*, 1805–1821.e8. https://doi.org/10.1016/j.stem.2021.05.001.
26. Zhang, X., Wei, X., Mei, Y., Wang, D., Wang, J., Zhang, Y., Li, X., Gu, Y., Peng, G., and Sun, B. (2021). Modulating adult neurogenesis affects synaptic plasticity and cognitive functions in mouse models of Alzheimer's disease. Stem Cell Rep. *16*, 3005–3019. https://doi.org/10.1016/j.stemcr.2021.11.003.
27. Song, J., Zhong, C., Bonaguidi, M.A., Sun, G.J., Hsu, D., Gu, Y., Meletis, K., Huang, Z.J., Ge, S., Enikolopov, G., et al. (2012). Neuronal circuitry mechanism regulating adult quiescent neural stem-cell fate decision. Nature *489*, 150–154. https://doi.org/10.1038/nature11306.
28. Song, J., Sun, J., Moss, J., Wen, Z., Sun, G.J., Hsu, D., Zhong, C., Davoudi, H., Christian, K.M., Toni, N., et al. (2013). Parvalbumin interneurons mediate neuronal circuitry-neurogenesis coupling in the adult hippocampus. Nat. Neurosci. *16*, 1728–1730. https://doi.org/10.1038/nn.3572.
29. Bao, H., Asrican, B., Li, W., Gu, B., Wen, Z., Lim, S.A., Haniff, I., Ramakrishnan, C., Deisseroth, K., Philpot, B., and Song, J. (2017). Long-range GABAergic inputs regulate neural stem cell quiescence and control adult hippocampal neurogenesis. Cell Stem Cell *21*, 604–617.e5. https://doi.org/10.1016/j.stem.2017.10.003.
30. Asrican, B., Wooten, J., Li, Y.D., Quintanilla, L., Zhang, F., Wander, C., Bao, H., Yeh, C.Y., Luo, Y.J., Olsen, R., et al. (2020). Neuropeptides modulate local astrocytes to regulate adult hippocampal neural stem cells. Neuron *108*, 349–366.e6. https://doi.org/10.1016/j.neuron.2020.07.039.
31. Yeh, C.Y., Asrican, B., Moss, J., Quintanilla, L.J., He, T., Mao, X., Cassé, F., Gebara, E., Bao, H., Lu, W., et al. (2018). Mossy cells control adult neural stem cell quiescence and maintenance through a dynamic balance between direct and indirect pathways. Neuron *99*, 493–510.e4. https://doi.org/10.1016/j.neuron.2018.07.010.
32. Oakley, H., Cole, S.L., Logan, S., Maus, E., Shao, P., Craft, J., Guillozet-Bongaarts, A., Ohno, M., Disterhoft, J., Van Eldik, L., et al. (2006). Intraneuronal beta-amyloid aggregates, neurodegeneration, and neuron loss in transgenic mice with five familial Alzheimer's disease mutations: potential factors in amyloid plaque formation. J. Neurosci. *26*, 10129–10140. https://doi.org/10.1523/JNEUROSCI.1202-06.2006.
33. Oddo, S., Caccamo, A., Shepherd, J.D., Murphy, M.P., Golde, T.E., Kayed, R., Metherate, R., Mattson, M.P., Akbari, Y., and LaFerla, F.M. (2003). Triple-transgenic model of Alzheimer's disease with plaques and tangles: intracellular Abeta and synaptic dysfunction. Neuron *39*, 409–421. https://doi.org/10.1016/s0896-6273(03)00434-3.
34. Ge, S., Yang, C.H., Hsu, K.S., Ming, G.L., and Song, H. (2007). A critical period for enhanced synaptic plasticity in newly generated neurons of

the adult brain. Neuron *54*, 559–566. https://doi.org/10.1016/j.neuron.2007.05.002.

35. Schmidt-Hieber, C., Jonas, P., and Bischofberger, J. (2004). Enhanced synaptic plasticity in newly generated granule cells of the adult hippocampus. Nature *429*, 184–187. https://doi.org/10.1038/nature02553.
36. Kim, E.J., Leung, C.T., Reed, R.R., and Johnson, J.E. (2007). In vivo analysis of Ascl1 defined progenitors reveals distinct developmental dynamics during adult neurogenesis and gliogenesis. J. Neurosci. *27*, 12764–12774. https://doi.org/10.1523/JNEUROSCI.3178-07.2007.
37. Madisen, L., Zwingman, T.A., Sunkin, S.M., Oh, S.W., Zariwala, H.A., Gu, H., Ng, L.L., Palmiter, R.D., Hawrylycz, M.J., Jones, A.R., et al. (2010). A robust and high-throughput Cre reporting and characterization system for the whole mouse brain. Nat. Neurosci. *13*, 133–140. https://doi.org/10.1038/nn.2467.
38. Zhu, H., Aryal, D.K., Olsen, R.H., Urban, D.J., Swearingen, A., Forbes, S., Roth, B.L., and Hochgeschwender, U. (2016). Cre-dependent DREADD (Designer Receptors Exclusively Activated by Designer Drugs) mice. Genesis *54*, 439–446. https://doi.org/10.1002/dvg.22949.
39. Ankney, J.A., Muneer, A., and Chen, X. (2018). Relative and absolute quantitation in mass spectrometry-based proteomics. Annu. Rev. Anal. Chem. (Palo Alto. Calif) *11*, 49–77. https://doi.org/10.1146/annurev-anchem-061516-045357.
40. Park, J., Chávez, A.E., Mineur, Y.S., Morimoto-Tomita, M., Lutzu, S., Kim, K.S., Picciotto, M.R., Castillo, P.E., and Tomita, S. (2016). CaMKII phosphorylation of TARPgamma-8 is a mediator of LTP and learning and memory. Neuron *92*, 75–83. https://doi.org/10.1016/j.neuron.2016.09.002.
41. Alkon, D.L., Sun, M.K., and Nelson, T.J. (2007). PKC signaling deficits: a mechanistic hypothesis for the origins of Alzheimer's disease. Trends Pharmacol. Sci. *28*, 51–60. https://doi.org/10.1016/j.tips.2006.12.002.
42. Yang, Y.R., Jung, J.H., Kim, S.J., Hamada, K., Suzuki, A., Kim, H.J., Lee, J.H., Kwon, O.B., Lee, Y.K., Kim, J., et al. (2017). Forebrain-specific ablation of phospholipase Cgamma1 causes manic-like behavior. Mol. Psychiatry *22*, 1473–1482. https://doi.org/10.1038/mp.2016.261.
43. Fuller, J.P., Stavenhagen, J.B., and Teeling, J.L. (2014). New roles for Fc receptors in neurodegeneration-the impact on Immunotherapy for Alzheimer's disease. Front. Neurosci. *8*, 235. https://doi.org/10.3389/fnins.2014.00235.
44. Qi, L.F., Liu, S., Liu, Y.C., Li, P., and Xu, X. (2021). Ganoderic acid A promotes amyloid-beta clearance (in vitro) and ameliorates cognitive deficiency in Alzheimer's disease (mouse model) through autophagy induced by activating Axl. Int. J. Mol. Sci. *22*, 5559. https://doi.org/10.3390/ijms22115559.
45. Toni, N., Laplagne, D.A., Zhao, C., Lombardi, G., Ribak, C.E., Gage, F.H., and Schinder, A.F. (2008). Neurons born in the adult dentate gyrus form functional synapses with target cells. Nat. Neurosci. *11*, 901–907. https://doi.org/10.1038/nn.2156.
46. Faulkner, R.L., Jang, M.H., Liu, X.B., Duan, X., Sailor, K.A., Kim, J.Y., Ge, S., Jones, E.G., Ming, G.L., Song, H., and Cheng, H.J. (2008). Development of hippocampal mossy fiber synaptic outputs by new neurons in the adult brain. Proc. Natl. Acad. Sci. USA *105*, 14157–14162. https://doi.org/10.1073/pnas.0806658105.
47. Drew, L.J., Kheirbek, M.A., Luna, V.M., Denny, C.A., Cloidt, M.A., Wu, M.V., Jain, S., Scharfman, H.E., and Hen, R. (2016). Activation of local inhibitory circuits in the dentate gyrus by adult-born neurons. Hippocampus *26*, 763–778. https://doi.org/10.1002/hipo.22557.
48. Luna, V.M., Anacker, C., Burghardt, N.S., Khandaker, H., Andreu, V., Millette, A., Leary, P., Ravenelle, R., Jimenez, J.C., Mastrodonato, A., et al. (2019). Adult-born hippocampal neurons bidirectionally modulate entorhinal inputs into the dentate gyrus. Science *364*, 578–583. https://doi.org/10.1126/science.aat8789.
49. Moore, A.N., Waxham, M.N., and Dash, P.K. (1996). Neuronal activity increases the phosphorylation of the transcription factor cAMP response element-binding protein (CREB) in rat hippocampus and cortex. J. Biol. Chem. *271*, 14214–14220. https://doi.org/10.1074/jbc.271.24.14214.
50. Silva, A.J., Kogan, J.H., Frankland, P.W., and Kida, S. (1998). CREB and memory. Annu. Rev. Neurosci. *21*, 127–148. https://doi.org/10.1146/annurev.neuro.21.1.127.
51. Sarlus, H., and Heneka, M.T. (2017). Microglia in Alzheimer's disease. J. Clin. Invest. *127*, 3240–3249. https://doi.org/10.1172/JCI90606.
52. Franco-Bocanegra, D.K., McAuley, C., Nicoll, J.A.R., and Boche, D. (2019). Molecular mechanisms of microglial motility: changes in ageing and Alzheimer's disease. Cells *8*, 639. https://doi.org/10.3390/cells8060639.
53. Gatt, A., Ekonomou, A., Somani, A., Thuret, S., Howlett, D., Corbett, A., Johnson, M., Perry, E., Attems, J., Francis, P., et al. (2017). Importance of proactive treatment of depression in Lewy body dementias: the impact on hippocampal neurogenesis and cognition in a post-mortem study. Dem. Geriatr. Cogn. Disord. *44*, 283–293. https://doi.org/10.1159/000484437.
54. Boldrini, M., Hen, R., Underwood, M.D., Rosoklija, G.B., Dwork, A.J., Mann, J.J., and Arango, V. (2012). Hippocampal angiogenesis and progenitor cell proliferation are increased with antidepressant use in major depression. Biol. Psychiatry *72*, 562–571. https://doi.org/10.1016/j.biopsych.2012.04.024.
55. Root, D.H., Zhang, S., Barker, D.J., Miranda-Barrientos, J., Liu, B., Wang, H.L., and Morales, M. (2018). Selective brain distribution and distinctive synaptic architecture of dual glutamatergic-GABAergic neurons. Cell Rep. *23*, 3465–3479. https://doi.org/10.1016/j.celrep.2018.05.063.
56. Ito, H.T., Moser, E.I., and Moser, M.B. (2018). Supramammillary nucleus modulates spike-time coordination in the prefrontal-thalamo-hippocampal circuit during navigation. Neuron *99*, 576–587.e5. https://doi.org/10.1016/j.neuron.2018.07.021.
57. Hashimotodani, Y., Karube, F., Yanagawa, Y., Fujiyama, F., and Kano, M. (2018). Supramammillary nucleus afferents to the dentate gyrus co-release glutamate and GABA and potentiate granule cell output. Cell Rep. *25*, 2704–2715.e4. https://doi.org/10.1016/j.celrep.2018.11.016.
58. Pedersen, N.P., Ferrari, L., Venner, A., Wang, J.L., Abbott, S.B.G., Vujovic, N., Arrigoni, E., Saper, C.B., and Fuller, P.M. (2017). Supramammillary glutamate neurons are a key node of the arousal system. Nat. Commun. *8*, 1405. https://doi.org/10.1038/s41467-017-01004-6.
59. Chen, S., He, L., Huang, A.J.Y., Boehringer, R., Robert, V., Wintzer, M.E., Polygalov, D., Weitemier, A.Z., Tao, Y., Gu, M., et al. (2020). A hypothalamic novelty signal modulates hippocampal memory. Nature *586*, 270–274. https://doi.org/10.1038/s41586-020-2771-1.
60. Li, Y., Bao, H., Luo, Y., Yoan, C., Sullivan, H.A., Quintanilla, L., Wickersham, I., Lazarus, M., Shih, Y.I., and Song, J. (2020). Supramammillary nucleus synchronizes with dentate gyrus to regulate spatial memory retrieval through glutamate release. eLife *9*, e53129. https://doi.org/10.7554/eLife.53129.
61. Farrell, J.S., Lovett-Barron, M., Klein, P.M., Sparks, F.T., Gschwind, T., Ortiz, A.L., Ahanonu, B., Bradbury, S., Terada, S., Oijala, M., et al. (2021). Supramammillary regulation of locomotion and hippocampal activity. Science *374*, 1492–1496. https://doi.org/10.1126/science.abh4272.
62. Gail Canter, R., Huang, W.C., Choi, H., Wang, J., Ashley Watson, L., Yao, C.G., Abdurrob, F., Bousleiman, S.M., Young, J.Z., Bennett, D.A., et al. (2019). 3D mapping reveals network-specific amyloid progression and subcortical susceptibility in mice. Commun. Biol. *2*, 360. https://doi.org/10.1038/s42003-019-0599-8.
63. Kim, E.J., Ables, J.L., Dickel, L.K., Eisch, A.J., and Johnson, J.E. (2011). Ascl1 (Mash1) defines cells with long-term neurogenic potential in subgranular and subventricular zones in adult mouse brain. PLoS One *6*, e18472. https://doi.org/10.1371/journal.pone.0018472.
64. Li, Y.D., Luo, Y.J., Xu, W., Ge, J., Cherasse, Y., Wang, Y.Q., Lazarus, M., Qu, W.M., and Huang, Z.L. (2021). Ventral pallidal GABAergic neurons control wakefulness associated with motivation through the ventral tegmental pathway. Mol. Psychiatry *26*, 2912–2928. https://doi.org/10.1038/s41380-020-00906-0.
65. Luo, Y.J., Li, Y.D., Wang, L., Yang, S.R., Yuan, X.S., Wang, J., Cherasse, Y., Lazarus, M., Chen, J.F., Qu, W.M., and Huang, Z.L. (2018). Nucleus accumbens controls wakefulness by a subpopulation of neurons expressing

dopamine D1 receptors. Nat. Commun. *9*, 1576. https://doi.org/10.1038/s41467-018-03889-3.

66. Huang, Y., Happonen, K.E., Burrola, P.G., O'Connor, C., Hah, N., Huang, L., Nimmerjahn, A., and Lemke, G. (2021). Microglia use TAM receptors to detect and engulf amyloid beta plaques. Nat. Immunol. *22*, 586–594. https://doi.org/10.1038/s41590-021-00913-5.

67. Roy, D.S., Arons, A., Mitchell, T.I., Pignatelli, M., Ryan, T.J., and Tonegawa, S. (2016). Memory retrieval by activating engram cells in mouse models of early Alzheimer's disease. Nature *531*, 508–512. https://doi.org/10.1038/nature17172.

68. Ryan, T.J., Roy, D.S., Pignatelli, M., Arons, A., and Tonegawa, S. (2015). Memory. Engram cells retain memory under retrograde amnesia. Science *348*, 1007–1013. https://doi.org/10.1126/science.aaa5542.

69. González Ibanez, F., Picard, K., Bordeleau, M., Sharma, K., Bisht, K., and Tremblay, M.È. (2019). Immunofluorescence staining using IBA1 and TMEM119 for microglial density, morphology and peripheral myeloid cell infiltration analysis in mouse brain. J. Vis. Exp. https://doi.org/10.3791/60510.

70. Tremblay, M.È., Zettel, M.L., Ison, J.R., Allen, P.D., and Majewska, A.K. (2012). Effects of aging and sensory loss on glial cells in mouse visual and auditory cortices. Glia *60*, 541–558. https://doi.org/10.1002/glia.22287.

71. Li, Y.D., Ge, J., Luo, Y.J., Xu, W., Wang, J., Lazarus, M., Hong, Z.Y., Qu, W.M., and Huang, Z.L. (2020). High cortical delta power correlates with aggravated allodynia by activating anterior cingulate cortex GABAergic neurons in neuropathic pain mice. Pain *161*, 288–299. https://doi.org/10.1097/j.pain.0000000000001725.

STAR★METHODS

KEY RESOURCES TABLE

REAGENT or RESOURCE	SOURCE	IDENTIFIER
Antibodies		
Anti-Rabbit c-Fos	Synaptic Systems	Cat# 7-80; RRID: 226003
Anti-Rabbit HA-tag	Cell Signaling Technology	Cat# 3724
Anti-Rabbit Ki67	Thermo Fisher Scientific	Cat# PA5-19462
Anti-Goat GFAP	Santa Cruz Biotechnology	Cat# sc-6170
Anti-Goat Sox2	Santa Cruz Biotechnology	Cat# sc-17320
Anti-Mouse NeuN	Millipore	MAB377
Anti-Goat DCX	Santa Cruz Biotechnology	Cat# sc-8066
Anti-Rabbit Aβ	Cell Signaling Technology	Cat#9888
Anti-rabbit Iba1	Wako	Cat#019-19741
Anti-rabbit pPLCg1	Thermo Fisher	Cat#BS-3343R
Anti-rabbit pCaMKII	Abcam	Cat#ab5683
Anti-rabbit pCREB	Cell Singling	Cat#9198
Anti-Rabbit RFP	Rockland	Cat# 600-401-379
Alexa Fluor 647 Donkey anti-Rabbit	Invitrogen	Cat # A32795
Alexa Fluor 647 Donkey anti-Goat	Invitrogen	Cat # A32849
Alexa Fluor 488 Donkey anti-Goat	Invitrogen	Cat # A32814
Alexa Fluor 488 Donkey anti-Rabbit	Invitrogen	Cat # A32790
Alexa Fluor 568 Donkey anti-Rabbit	Invitrogen	Cat # A10042
Bacterial and virus strains		
AAV5- CaMKII-eYFP	UNC Vector Core	N/A
AAV5- CaMKII-mCherry	UNC Vector Core	N/A
AAV5-CaMKII-ChR2-mCherry	UNC Vector Core	N/A
AAV5-CaMKII-ChR2-eYFP	UNC Vector Core	N/A
AAV9- hsyn-DIO-GCaMP7	UNC Vector Core	Cat #104492
AAV2-retro-Cre	Addgene	Cat #55636
AAV5-DIO-hM3Dq-mCherry	Addgene	Cat344361
Retrovirus (RV)-CAG-HA-Cre	University of North Carolina at Chapel Hill	Dr. Kimberly D Ritola
Chemicals, peptides, and recombinant proteins		
Bicuculline	Tocris	Cat #0131
TTX	Tocris	Cat #1078
Thio-S	Sigma	Cat #MKCH408
Pierce™ Quantitative Colorimetric Peptide Assay	Thermofisher	23275
High-Select™ Fe-NTA Phosphopeptide Enrichment Kit	Thermofisher	A32992
CNO	NIH	Cat #C-929
Deposited data		
PXD034176	ProteomeXchange	http://www.ebi.ac.uk/pride/archive/projects/PXD034176
Experimental models: Organisms/strains		
Mouse: Ascl1CreER (B6, Ascl1$^{tm1.1(cre/ERT2)Jejo}$) mice	Jackson laboratory	Stock No: 012882
Mouse: Ai9 (B6, Gt(ROSA)26Sor$^{tm9(CAG\text{-}tdTomato)Hze}$) mice	Jackson laboratory	Stock No: 007909
Mouse: hM3Dq-flox (B6, Tg(CAG-CHRM3*,-mCitrine)1Ute) mice	Jackson laboratory	Stock No: 026220

(*Continued on next page*)

Continued

REAGENT or RESOURCE	SOURCE	IDENTIFIER
Mouse: 5xFAD	Jackson laboratory	Stock No. 008730
Mouse:3xTg-AD	Jackson laboratory	Stock No: 004807
Software and algorithms		
MATLAB R2014b	Mathworks	RRID:SCR_001622
Imaris	Bitplane	RRID: SCR_007370
FIJI	ImageJ	RRID: SCR_002285
pClamp	Molecular Devices	RRID: SCR_011323
Olympus FluoView	Olympus	RRID: SCR_014215
MaxQuant software version 1.6.10.43	Max Planck Institute	https://maxquant.net/perseus/
UniProt human protein sequence database	UniProt	UP000005640
Prism	Graphpad	RRID:SCR_002798
Adobe Illustrator	Adobe	www.adobe.com

RESOURCE AVAILABILITY

Lead contact

Further information and requests for resources and reagents should be directed to and will be fulfilled by the lead contact, Juan Song (juansong@email.unc.edu).

Materials availability

This study did not generate new unique reagents.

Data and code availability

Proteomics data have been deposited at ProteomeXchange and are publicly available as of the date of publication. Accession numbers are listed in the key resources table. This paper does not report the original codes. Any additional information required to reanalyze the data reported in this paper is available from the lead contact upon request.

EXPERIMENTAL MODEL AND SUBJECT DETAILS

Experimental animals

Single, double, or triple transgenic mice (6-14 weeks, males and females) were used for all experiments from the following genetically modified mouse lines: Ascl1CreERT2[36,63] (B6), and Ai9 (B6) mice and 5×FAD (B6) mice were obtained from the Jackson laboratory; hM3Dq-flox[38] (R26-LSL-Gq-DREADD, B6) mice were obtained from Bryan Roth's lab at the University of North Carolina at Chapel Hill. Ascl1CreERT2 mice were mated to Ai9 or hM3Dq mice to get Ascl1-CreER::Ai9 or Ascl1CreER::hM3Dq mice. Then, Ascl1-CreER::Ai9 or Ascl1-CreER::hM3Dq mice were mated with 5×FAD mice to get Ascl1CreER::Ai9::5×FAD mice or Ascl1-CreER::hM3Dq::5×FAD mice. The Ascl1CreER$^{+/-}$::Ai9$^{+/-}$ littermates or hM3Dq::5×FAD littermates were used as control, based on the design of different experiments. Only Ascl1CreER heterozygous mice were used in the experiments. The aged triple-transgenic mice 3×Tg-AD[33] were the gifts from Dr. Leon Coleman at UNC. Both male and female AD mice were used in this study and gender was matched in different groups. No immune deficiencies or other health problems were observed in these lines, and all animals were experimentally and drug-naive before use. Animals were group-housed and bred in a dedicated husbandry facility with 12/12 hour light-dark cycles with food and water ad libitum and under veterinary supervision. Behavior tests were performed in the light phase. Animals subjected to surgical procedures were moved to a satellite housing facility for recovery with the same light-dark cycle. All procedures were conducted in accordance with the NIH Guide for the Care and Use of Laboratory Animals and with the approval of the Institutional Animal Care and Use Committee at the University of North Carolina at Chapel Hill (UNC).

Choice of the mouse model

In our study, we used a well-established AD mouse line, 5×FAD mice (C57BL6 background), which expresses human APP and PSEN1 transgenes with a total of five AD-linked mutations: the Swedish (K670N/M671L), Florida (I716V), and London (V717I) mutations in APP, and the M146L and L286V mutations in PSEN1.[32] Most of the current AD transgenic mouse models are generated by the overexpression of mutation(s) related to familial AD (FAD). While the 5×FAD mouse model expresses rare early-onset FAD mutations, the pathological features found in the brains of 5×FAD mice are common to all forms of AD. Therefore, we believe that the results of our studies are also relevant for generalized AD pathology (beyond that of early-onset FAD). We chose 5×FAD mice, which show faster AD progression than other AD mouse models, based on our goal of investigating whether chronic stimulation of SuM neurons during early-stage AD when AHN is mildly impaired is beneficial for AHN and memory performance at later AD stages. Specifically,

our chronic SuM stimulation paradigm lasts 32 days, and we intend to address whether 32-d SuM stimulation is sufficient to improve hippocampal neurogenesis. 5×FAD mice are ideal for this purpose, as within this time frame (from 3.5 to 4.5 months of age), 5×FAD mice exhibit progressive impairment of hippocampal neurogenesis, ranging from mild impairment at early AD stages to more severe impairment at later AD stages.

To avoid the bias of the fast 5×FAD mouse model, we also used the triple-transgenic mice 3×Tg-AD to validate the key neurogenesis and behavioral results under the same SuM stimulation paradigm. 3×Tg-AD mice harbor expression of human transgenes with familial mutations associated with AD, including PSEN1 M146V, APP Swedish, and MAPT P301L. Importantly, 3×Tg-AD mice have slower AD pathology, compared to 5xFAD mice.

METHOD DETAILS

Stereotaxic surgery

Mice were anesthetized under 1.5−2 % isoflurane in oxygen at 0.8 LPM flow rate. The virus was injected by microsyringe (Hamilton, 33GA) and microinjection pump (Harvard Apparatus), at a rate of 30−50 nl/min with the following coordinates: AAVs were injected unilaterally into the lateral SuM (anteroposterior (AP): −2.4 mm, mediolateral (ML): ±0.6 mm, dorsoventral (DV): −4.85 mm) or the DG (AP: −2.0 mm, ML: ±1.4 mm, DV: −2.0 mm). A total of 150−250 nl of the virus was delivered to each site, and the needle was left in the site for at least 10 min to permit diffusion. All coordinates were based on values from 'The Mouse Brain Stereotaxic Coordinates'.

For *in vivo* fiber photometry recording, retroAAV2-Cre (Addgene) was injected into DG, and AAV5-DIO-GCaMP7 was injected into SuM, respectively. Unilateral optic fibers (Newdoon Inc, O.D.: 1.25 mm, core: 200 μm, NA: 0.37) were implanted in the SuM at AP: −2.4 mm, ML: + 0.6 mm, DV: −4.85 mm.

For *in vivo* optogenetics, unilateral optic fibers (Newdoon Inc, O.D.: 1.25 mm, core: 200 μm, NA: 0.37) above the SuM at AP: −2.4 mm, ML: + 0.6 mm, DV: −4.5 mm. We only unilaterally stimulated SuM neurons because SuM neurons send almost equal projections to the bilateral DG. After 3 weeks of recovery, mice were used for *in vivo* optogenetic stimulation.

To activate SuM enhanced ABNs in 3×Tg-AD mice, AAV-CaMKII-ChR2-YFP or control virus AAV-CaMKII-YFP was injected into SuM. After 2 weeks, Retrovirus (RV)-HA-Cre (1 μl) mixed with AAV-DIO-hM3Dq-mCherry (200 nl) was injected into both dorsal (AP: −2.0 mm, ML: ± 1.45 mm, DV: −2.0 mm) and ventral (AP: −3.65 mm, ML: ± 2.60 mm, DV: −3.25 mm)DGs, with fiber implantation above SuM. One day after optogenetic stimulation, behaviors were tested with CNO injection to activated ABNs.

In terms of the quality control for our data, mice with off-target viral injection/expression in SuM were excluded from analysis after post hoc examination of fluorescence expression. The coverage of the injection site in lateral SuM was examined to control inter-animal variability.

Fiber photometry recording and analysis

After 3 weeks of surgery, fiber photometry recording was carried out by using a commercial device (RWD life science, Shenzhen, China) as previously described.[60,64,65] In brief, 470 nm and 410 laser beams first launched into the fluorescence cube, then launched into the optical fibers. 410 laser was used for motion control. The GCaMP and control emission fluorescence was collected by the camera at 20 Hz. The *in vivo* recordings were carried out in an open-top home cage (21.6 × 17.8 × 12.7 cm) for 10 minutes. We derived the value of the photometry signal F as F_{470}/F_{410}, calculating $\Delta F/F = (F - F_0) / F_0$, where F_0 is the median of the photometry signal. Only calcium signal over 3 SD was treated as events. The average of 10 peak $\Delta F/F$ and the number of events per minute for each mouse were analyzed.

Chemical administration and optogenetic/chemogenetic stimulation protocol

For lineage-tracing experiments, 473 nm blue light stimulation at 10 Hz, 5 ms, 30 s/5 minutes was given as below: For 3-day post tamoxifen injection (dpi), blue light stimulations were given 8 hours/day for 3 days with tamoxifen at 80 mg/kg i.p. injections (3 shots in total). Mice were perfused on day 3 after the last tamoxifen injection. For 32 dpi experiments, blue light was given for 8 hours for the first 3 days with 80 mg/kg tamoxifen i.p. injection. From day 4 to 32, blue light stimulations were given for 2 hours/day, and mice were perfused on day 32 immediately after light stimulation. For behavior tests after chronic SuM stimulation, mice were tested from day 33 (1 day after the last optogenetic stimulation) to avoid acute effects from SuM activation.

For chemogenetic activation of DG newborn neurons, CNO 0.5 mg/kg was administered to AM3-AD and M3-AD mice via i.p. injection, 30−60 min before memory retrieval or emotional behavior tests, respectively. For chronic SuM-stimulated mice, behavior tests were performed from day 33 (1 day after the last optogenetic stimulation) to avoid acute effects from SuM activation.

Immunohistochemistry (IHC)

Mice were perfused and then brain samples were fixed in 4% paraformaldehyde (PFA) for 24 hours, followed by 30% sucrose for 2−3 days until they were fully submerged. Brains slices from frozen section at a thickness of 40 μm and stored in an anti-freeze solution at −20°C for further usage. For all staining, sections were pretreated as following; 5-minute incubations in PBS, 3 x 5-minute incubations in 1 mg/ml Sodium borohydride in PBS, then 2-hour incubations in 0.3% Triton-X in PBS (PBST), then 2-hour incubations in 0.1% PBST containing 5% donkey serum. Sections were incubated in primary antibody solution in 0.1% PBST and kept at 4 degrees for 48 hours with shaking. After primary incubation, the sections went through 3 x 20-minute wash steps in 0.1% PBST. Sections were then transferred to a secondary antibody solution in 0.1% PBST for 2 hours at 24 degrees with shaking. Sections were

washed 3 x 30-minute in 0.1% PBST with 1 μM DAPI solution included on the third wash step. Finally, sections were mounted onto charged glass slides using Diamond prolong gold mounting media (Thermo Fisher Scientific, P36961) and a no.1.5 glass coverslips (Electron Microscopy Sciences, #72204-02).

For c-Fos labeling, mice were perfused 90 minutes after CNO injection. A rabbit c-Fos antibody (Synaptic System, #226003) was used at 1:1000. For Aβ and GFAP staining, a rabbit Aβ antibody (Cell Signaling Technology, #9888) was used at 1:1000; for GFAP staining, a goat GFAP antibody (Santa Cruz Biotechnology, #sc33673) was used at 1:1000. For HA-tag staining, a rabbit HA-tag antibody (Cell Signaling Technology, #3724) was used at 1:500 to label the Ascl1-hM3Dq cells. For NeuN and DCX staining, a mouse NeuN antibody (Millipore, #MAB377) and a rabbit DCX antibody (Cell Signaling Technology, #4604) were used at 1:500. For Iba1 staining, a rabbit Iba1 antibody (Wako, #019-19741) was used at 1:1000 after antigen retrieval. For spine counting, the fluorescence of tdTomato was raised by anti-RFP staining. For LTP pathway validation, anti-rabbit pPLCg1 (Thermo Fisher, #BS-3343R), anti-rabbit pIP3R (Boster, #A01465S1598), anti-rabbit pCaMKII (Abcam, #ab5683), anti-rabbit pCREB (Cell Singling, #9198) antibody was used at 1:500, respectively.

Image analysis

All image analyses were performed blind to the experimental group. Confocal images containing regions of interests were taken by confocal microscopy (Olympus FLUOVIEW3000), and then loaded into ImageJ (FIJI). Cell counting in DG was performed following stereological methods adopted in our previous publications.[22,27–31] Specifically, we quantified 5 sections/per mouse spanning from anterior to posterior. The cell number of each DG was divided by the DG volume (area of the GCL (by DAPI) /slice × thickness of the sections) to get the cell density counts. Cells were counted using the Cell Counter plugin in ImageJ. Then the average density of 5 sections was calculated for each animal. For lineage analysis, cells were counted as below: (1) For 3 dpi experiments: the total number of tdTomato+ and Ki67+/tdTomato+ cells were counted per section. (2) For 32 dpi experiments, the total number of tdTomato+, tdTomato+NeuN+, and tdTomato+DCX+ neurons were counted per section. For Ascl1-hM3Dq mice, HA-tag labeled cells were counted.

For microglial-amyloid beta colocalization analysis, Aβ and Iba1 staining images were taken by confocal microscopy (Olympus FLUOVIEW3000) under a × 60 objective, 1 × zoom in, XY-resolution 0.4975 mm/pixel, Z-resolution 0.8 μm/slice and then loaded into Imaris (version 9.9.1). A region of interest (ROI) surface was drawn around the DG, and their volumes were recorded. Channel fluorescence was masked to the region (setting outside voxel to 0). ROI Aβ and Iba1 volume were measured after thresholding to exclude the background noise. Next, using the 'colocalization' function, ROI Aβ and Iba1 interaction was determined using the same intensity thresholds for the Aβ channel and Iba1 channel that was used to create their volumetric surfaces. The volume of co-localization was normalized to total ROI Iba1 volume, which is the maximum volume that could be considered colocalized.[66]

For Spine density analysis, dendritic spine was analyzed for newborn neurons (32 dpi) labeled by tdTomato fluorescence. DG sections were obtained from ChR2-YPF and YFP control Ascl1CreER-Ai9 mice 32 days post tamoxifen injection. The tdTomato signal was taken by confocal microscopy (Olympus FLUOVIEW3000) under a × 60 objective, 3 × zoom in, XY-resolution 0.4975 mm/pixel, Z-resolution 0.5 μm/slice. Four mice per experimental group were analyzed for dendritic spines. For each mouse, 20 dendritic fragments of 10-μm length were quantified (n = 80 fragments per group). Distal dendritic fragments in the middle-to-outer molecular layer (ML) were selected. To compute spine density, the number of spines counted on each fragment was normalized by the cylindrical approximation of the surface of the specific fragment.[67,68] Experiments were conducted blind to the experimental group. Researcher 1 imaged dendritic fragments and randomized images, while researcher 2 performed manual spine counting.

Microglia morphology analysis was performed based on previous studies.[69,70] Microglia was immunofluorescence labeled by antibody (anti-Iba-1, 1:1,000, Wako #019-19741). Images were taken by confocal microscopy (Olympus FLUOVIEW3000) under a × 60 objective, 1 × zoom in, XY-resolution 0.4975 mm/pixel, Z-resolution 0.5 μm/slice, and then loaded into Image to count microglia number. Microglia density was normalized by DG hilus volume. Microglial somas and branches were outlined manually in ImageJ and the morphological index was calculated as soma area/arborization area. In total, 20 microglia from 4 slices were counted for each mouse and the average value of each mouse for a total of 5 mice/each group were compared.

Behavioral tests

Contextual fear conditioning (CFC)

Contextual fear conditioning experiments were carried out in a commercial fear conditioning system (Med Associate) as previously described.[22] On Day 1, mice were habituated in the behavioral context for 3 min, followed by two foot shocks (0.65 mA, 2 s) delivered at 180 s and 240 s. Mice remained in the behavior chamber for 80 s after the second foot shock and then returned to their home cages. Memory retrieval was performed at 2 hours, 24 hours, and 1 week after encoding in the conditioned context (A, grid floors, opaque ceilings, white lighting) or a different context (B, white plastic floors, curved wall with visual cues, white lightning, B) for 5 min to recall memory. To minimize the animal number, the same cohort of mice was used for CFC tests at different retrievals. Each mouse was injected with CNO 2 times for the CFC test at 24h, and 7 days after training. Behavior videos were recorded with VideoFreeze software and the freezing level was automatically analyzed by the software.

Novel position recognition (NPR)

NPR tests were performed as previously described.[60] In brief, the encoding phases were identical for the NPR task and comprised a 10-minute interval during which the mice were allowed to explore two identical objects in the open field. After 24 hours, memory retrieval was tested. One of the two objects from the encoding phase was moved to a different location. At each test,

mice had 5 minutes to explore the arena. Only the mice that showed no preference for objects in the encoding phase were included in the behavior analysis. Object exploration was considered whenever the mouse sniffed the object or touched the object while looking at it (when the distance between the nose and the object was less than 1 cm). Times were converted into a discrimination ratio according to the general formula: (time at novel − time at old)/(time at old + time at novel), where 'novel' refers to the novel position object.

Open field (OF) test

The OF test apparatus was a Plexiglas-squared arena (45 × 45 cm) with gray walls (40-cm high) and an open roof. Mice were gently placed in the center of the field, and movement was recorded for 5 min with a video-tracking system. The time spent in the center of the arena (defined as a 25 × 25 cm zone in the center of the apparatus) was measured.[64,71] Locomotion and time spent in the central area were analyzed by EthoVision XT (Noldus, Netherlands).

Forced swimming (FS)

The FS test apparatus consisted of an acrylic cylinder (with a diameter of 20 cm and height of 30 cm) filled with water to a depth of 20 cm and maintained at 23 ± 1 °C. Each mouse was subjected to a 5 min videotaped swimming trial and subsequently analyzed by two independent observers who were blinded to the treatment. Time of immobility was reported as the mouse remained immobile during the test session. After each trial, the apparatus was filled with fresh water.

Zero-maze (ZM)

The ZM test apparatus was comprised of a 6 cm wide white ring, 45 cm outer diameter, containing four equal quadrants of alternating walled (closed) or unwalled (open) sections, and the entire ring was elevated to a height of 40 cm. Animal were placed in the closed section at the start of the 5-min session. The following parameters were recorded and the time spent in the open sections was counted. After each trial, the maze was cleaned with a damp tissue containing 75% ethanol.

Sample preparation for global expression analysis and mass spectrometry analysis

Peptides, generated from M3AD (3x), AM3AD (2x), ChR2-AM3AD (3x) and mch-AM3AD (3x) were labeled with isobaric stable tandem mass tags (TMT) following manufacture instruction. The mixture of labeled peptides was fractionated into 15 fractions on C18 stage tip with buffer 10 mM Trimethylammonium bicarbonate (TMAB), pH 8.5 containing 5 to 50% acetonitrile. Dried peptides were dissolved in 0.1% formic acid, 2% acetonitrile. 0.5 μg of peptides of each fraction was analyzed. Analytical separation of all peptides was achieved with 140-min gradient. A linear gradient of 5 to 10% buffer B over 5 min, 10% to 31% buffer B over 100 min, 31% to 75% buffer B over 15 min was executed at a 250 nl/min flow rate followed a ramp to 100%B in 1 min and 19-min wash with 100%B, where buffer A was aqueous 0.1% formic acid, and buffer B was 80% acetonitrile and 0.1% formic acid. MS experiments were also carried out in a data-dependent mode with full MS with a resolution of 120,000 followed by high energy collision-activated dissociation-MS/MS of the top 15 most intense ions with a resolution of 45,000 at *m/z* 200. High energy collision-activated dissociation-MS/MS was used to dissociate peptides at a normalized collision energy of 32 eV in the presence of nitrogen bath gas atoms. Dynamic exclusion was 45 seconds. Every fraction was subject to three technical LC-MS replicates.

Phosphorylated peptide enrichment

Proteins of mouse hippocampus (3 mice each group) tissue was extracted with a buffer of 8 M Urea, 50 mM Tris-HCl pH 8.0. Proteins in the lysate were reduced with dithiothreitol (5 mM final) for 30 min at room temperature and alkylated with iodoacetamide (15 mM final) for 45 min in the dark at room temperature. Samples were diluted 4-fold with 25 mM Tris-HCl pH 8.0, 1 mM CaCl2, and digested with trypsin at 1:100 (w/w, trypsin : protein) ratio overnight at room temperature. Peptides were desalted on C18 cartridge (Waters). Peptide concentration was measured with Pierce™ Quantitative Colorimetric Peptide Assay (Thermofisher). 1 mg of each peptide sample was used for phosphor-enrichment with High-Select™ Fe-NTA Phosphopeptide Enrichment Kit (Thermo Fisher) following the manufacture instruction. There were three biological samples for each condition.

Mass spectrometry analysis

Dried phosphorylated peptides were dissolved in 0.1% formic acid, 0.3% TFA, and 2% acetonitrile. 0.5 μg of phosphor-peptides was analyzed on a Q-Exactive HF-X coupled with an Easy nanoLC 1200 (Thermo Fisher Scientific). Peptides were loaded onto a nanoEase MZ HSS T3 Column (100Å, 1.8 μm, 75 μm x 250 mm, Waters). Analytical separation of all peptides was achieved with a 100-min gradient. A linear gradient of 5 to 30% buffer B over 75 min, 30% to 45% buffer B over 15 min was executed at a 300 nl/min flow rate followed by a ramp to 100%B in 1 min and 9-min wash with 100%B, where buffer A was aqueous 0.1% formic acid, and buffer B was 80% acetonitrile and 0.1% formic acid. LC-MS experiments were also carried out in a data-dependent mode with full MS (externally calibrated to a mass accuracy of <5 ppm and a resolution of 60,000 at *m/z* 200) followed by high energy collision-activated dissociation-MS/MS of the top 15 most intense ions with a resolution of 15,000 at *m/z* 200. High energy collision-activated dissociation-MS/MS was used to dissociate peptides at a normalized collision energy of 27 eV in the presence of nitrogen bath gas atoms. Dynamic exclusion was 30 seconds. Each sample was subjected to two replicate technical LC-MS analyses.

Raw proteomics data processing and analysis

Mass spectra were processed, and peptide identification was performed using the MaxQuant software version 1.6.10.43 (Max Planck Institute, Germany). Protein database searches were performed against the UniProt human protein sequence database (UP000005640). A false discovery rate (FDR) for both peptide-spectrum match (PSM) and protein assignment was set at 1%. Search parameters included up to two missed cleavages at Lys/Arg on the sequence, phosphorylation of tyrosine, serine, and threonine, oxidation of methionine, and protein N-terminal acetylation as dynamic modifications. Carbamidomethylation of cysteine residues was considered as a static modification. Peptide identifications are reported by filtering of reverse and contaminant entries and assigning to their leading razor protein. Data processing and statistical analysis were performed on Perseus (Version 1.6.0.7). The

missing values of intensity were replaced with a constant that is the lowest non-zero value of all data. Two-sample tests were performed for comparing two groups. A p-value of 5% was used to report statistically significant abundance fold-changes. The canonical pathways were analyzed by Ingenuity Pathway Analysis (IPA) (http://www.ingenuity.com).

Slice preparation

4.5- to 5-month-old 5×FAD mice, AM3-AD mice, and M3-AD mice were used for LTP recordings. Mice were anesthetized and perfused transcardially with ice-cold modified artificial cerebral spinal fluid (ACSF) saturated with 95% O2 and 5% CO2 and containing (in mM):225 sucrose, 2.5 KCl, 7 glucose, 1.25 NaH2PO4, 24 NaHCO3, 2 Na-pyruvate, 0.4 ascorbic acid, 7 MgSO4, and 0.5 CaCl2 (pH 7.35, osmolarity 300-310 mOsM). Brains were then rapidly removed, and acute transverse hippocampal slices (350 μm thick) were cut using a vibratome (VT1200, Leica) in ice-cold modified ACSF. Next, slices were transferred to a holding chamber containing standard recording ACSF (in mM): 125 NaCl, 2.5 KCl, 11 glucose, 1 NaH2PO4, 26 NaHCO3, 2 Na-pyruvate, 1.3 MgSO4, and 2.5 CaCl2 (pH 7.35, osmolarity 300-310 mOsM), and allowed to recover for 30 min at 34 °C. Then, slices were maintained at room temperature for at least 60 min before recording.

Long-term potentiation (LTP) recording

Slices were withdrawn from the holding chamber as needed and placed in a recording chamber, where they were continuously perfused at a rate of 2 ml/min with standard ACSF. The recording chamber was kept at a temperature of 30 ± 1 °C by an automatic temperature controller (Warner TC-324B). Field excitatory postsynaptic potentials (fEPSPs) were evoked in the CA1 stratum radiatum by stimulation of Schaffer collaterals with a concentric bipolar stimulating electrode (30200, FHC) and recorded with ACSF-filled glass pipettes (2-4 MΩ) using Axoclamp-700B amplifiers and a Digidata 1440A analogue-to-digital converter (Molecular Devices, CA). Basal fEPSPs were evoked by a brief pulse (100-μs) of constant current delivered by stimulus isolation unit (ISO-Flex, AMPI, Israel) every 30 s. fEPSPs were filtered at 1 kHz and digitized at sampling rates of 10 kHz with a DigiData 1440A (Axon Instruments). Data were acquired and analyzed with pClamp10.7 software (Molecular Devices, CA). The pulse intensity was adjusted to elicit approximately 40% of the maximum response (fEPSP slope). The strength of synaptic transmission was determined by measuring the initial (20%–70% of rising phase) slope of the fEPSP.

CNO 10 μM (dissolved in ACSF, containing 0.1% DMSO) was bath applied during the recording. A 20-min stable baseline was recorded prior to LTP induction. LTP was induced with three theta-burst stimulation, which is four pulses at 100 Hz, repeated three times with a 200-ms interval. Responses were recorded for an hour following the last stimulation. The average of fEPSP slopes during the last 10 min prior to the induction of LTP was taken as the baseline, and the values of fEPSP slope measured during 50-60 min after LTP induction was used for analysis. All values were normalized to the averaged baseline value.

QUANTIFICATION AND STATISTICAL ANALYSIS

Data are reported and presented as the mean ± SEM. No statistical methods were used to pre-determine sample sizes but our sample sizes are similar to those reported in previous publications.[22,60,64,65] Animals or data points were not excluded and each experiment was repeated 2 times. Both behavioral analysis and cell counting were performed blinded to the conditions of the experiments. To compare the cell density, spine density, discrimination ratios, freezing percent, and other behavioral tests in different groups, we used unpaired *t*-tests or paired *t*-tests. In multi-group comparison, a one-way or two-way ANOVA was used, followed by Tukey's post-hoc test. Testing was always performed two-tailed with $\alpha = 0.05$. 'n.s' indicates no significant difference ($P > 0.05$). Statistical analyses were performed in GraphPad Prism8.